GEOLOGICA CARPATHICA, FEBRUARY 2013, 64, 1, 3–22 doi: 10.2478/geoca-2013-0001

Provenance of Paleozoic very low- to low-grade metasedimentary rocks of South Tisia (Slavonian Mountains, Radlovac Complex, Croatia)

VANJA BIŠEVAC[1], ERWIN KRENN[3], FRITZ FINGER[3], BORNA LUŽAR-OBERITER[2] and DRAŽEN BALEN[1]

[1]Institute of Mineralogy and Petrology, Department of Geology, Faculty of Science, University of Zagreb, Horvatovac 95, HR-10000 Zagreb, Croatia; vabisevac@geol.pmf.hr
[2]Institute of Geology and Paleontology, Department of Geology, Faculty of Science, University of Zagreb, Horvatovac 102, HR-10000 Zagreb, Croatia
[3]Division of Mineralogy, Department of Materials Engineering and Physics, University of Salzburg, Hellbrunnerstrasse 34, 5020 Salzburg, Austria

(Manuscript received April 23, 2012; accepted in revised form June 13, 2012)

Abstract: Monazite age dating, detrital heavy mineral content and whole-rock geochemistry provided insight into the provenance, depositional history and paleogeological setting of the Radlovac Complex very low- to low-grade metasedimentary rocks (South Tisia, Slavonian Mountains, Croatia). Electron microprobe based Th-U-Pb dating of detrital monazite indicates a Variscan age of the protolith (330±10 Ma). The detrital heavy mineral assemblages of representative metasedimentary rocks are dominated by apatite, zircon, tourmaline and rutile accompanied by minor quantity of epidote/zoisite, monazite and titanite. Judging from the heavy mineral assemblage, felsic igneous rocks served as the source material. This is consistent with the major and trace element spectrum of studied metasedimentary rocks characterized by high concentration of Th, high L+MREEs and high ratios of La/Sc, Th/Sc, La/Co, Th/Co and Th/Cr. The occurrence of magmatic monazite, zircon and xenotime and the absence of metamorphic heavy minerals suggest that granitoids, migmatites and migmatitic gneisses served as one major source for the metapsammites. Such rock types are commonly exposed in the Papuk Complex of the older surrounding complexes, while the Psunj Complex also contains metamorphic rocks. This is in good correlation with the monazite ages presented here which fits better with ages of Papuk Complex representative rocks than with those of the Psunj Complex known from the literature. Overall, data show that the Radlovac Complex represents the detritus of the local Variscan crust characterized by granitoid bodies, migmatites and migmatitic gneisses typical for the Papuk Complex.

Key words: South Tisia, Slavonian Mts, Radlovac Complex, metasedimentary rocks, geochemistry, geochronology, provenance, heavy minerals, detrital monazite.

Introduction

The primary role of provenance studies is to reconstruct the history of sedimentary rock and to interpret the rock-assemblage of the source area (Weltje & von Eynatten 2004). To this end, the combination of bulk rock and single grain analytical approaches has been shown to provide comprehensive insights into the provenance of sedimentary rocks (e.g. von Eynatten 2003; Meinhold et al. 2007; Mikes et al. 2008). Although processes of weathering and erosion, as well as metamorphism, commonly alter and remove valuable provenance information, certain trace element indicators are sufficiently resilient to survive such destructive processes. Many studies, both on sedimentary (e.g. Bathia 1985; Bathia & Crook 1986; McLennan et al. 1993), and metasedimentary (e.g. Slack & Höy 2000; Augustsson & Bahlburg 2008) rocks, have shown that geochemical data can be successfully used to study the composition and reveal the geotectonic environment of source rocks, especially when coupled with petrography and heavy mineral assemblages. Furthermore, various studies, where analysis is focused on one particular mineral species, are less affected by the aforementioned processes and are able to reveal specific provenance related information (e.g. Hallsworth et al. 2000; Willner et al. 2001; von Eynatten & Wijbrans 2003; Zack et al. 2004).

From the Radlovac Complex, which occupies the highest structural position of all Variscan complexes in the Slavonian Mountains (Jamičić 1983, 1988; Jamičić & Brkić 1987; Jamičić et al. 1987), no provenance study has been carried out although some authors contributed to the origin of the Radlovac Complex (e.g. Brkić et al. 1974; Jamičić 1988). In this study we present results from the Radlovac Complex which comprises very low- to low-grade metasedimentary rocks with intrusions of metabasic rocks (Jamičić 1983, 1988; Pamić & Jamičić 1986). We present results from mineral and whole-rock chemical analysis of 16 selected fresh samples including 8 metapelites and 8 metapsammites. For comparison, additional 7 representative samples from the surrounding igneous-metamorphic complexes were used for testing possible relations and the provenance model of Jamičić (1988). The analytical data include petrography, heavy mineral composition analyses, zircon typology, chemi-

cal composition and Th-U-Pb chemical age dating of monazite and xenotime and whole-rock geochemistry including major, trace and REE element composition. The aim of this study is to provide more detailed insight into the provenance, depositional history and paleogeological setting of the Radlovac Complex metasedimentary rocks and to provide a good basis for correlation with other similar very low- to low-grade metamorphic complexes within Tisia.

Geological setting

Tisia is regarded as a microcontinent that broke off from the southern margin of Variscan Europe during the opening of the Tethys (Géczy 1973; Fülöp et al. 1987; Tari & Pamić 1998; Haas et al. 2000; Pamić et al. 2002; Stampfli et al. 2002; Haas & Péró 2004; Schmid et al. 2008). Following a complex drift history, Tisia became incorporated into the Alpine fold belt in the Cretaceous (Csontos 1995; Márton 2000, 2001). Tisia is built up by three southward dipping Alpine nappe systems (Mecsek, Villány-Bihor and Békés-Codru) (Fig. 1), each comprising igneous and metamorphic basement rocks and post-Variscan overstep sequences (Haas & Péró 2004; Csontos & Vörös 2004; Schmid et al. 2008). According to Schmid et al. (2008) the Slavonian Mountains belong to the Villány-Bihor nappe system (Fig. 1) and represent rare basement outcrops of Tisia (Pamić et al. 1996; Pamić & Jurković 2002).

Following Jamičić (1983, 1988) three tectono-metamorphic complexes can be defined in the Slavonian Mountains: Psunj Complex (PsC), Papuk Complex (PaC) and Radlovac Complex (RC). The RC, which is the target of this research, consists of very low- to low-grade metamorphic sequences largely composed of metapelites (slates and subordinate phyllites), metapsammites (metagreywackes) and metaconglomerates deposited in the shallow marine environment (Jamičić 1988). According to Pamić & Jamičić (1986) the deepest part of RC is represented by violet, and grey to silverish white schistose metagreywackes which grade into quartz metaconglomerates in some places (Fig. 2). The middle parts are made of violet and greyish finer-grained schistose metagreywackes (Fig. 2) interlayered with dark greyish slates containing Westphalian microflora. The highest part of the Radlovac Complex consists mostly red to brownish slates and phyllites (Fig. 2) rarely interlayered by fine-grained metapsammites. Based on the structural and paleofloristic data Jamičić (1988) assumed that the RC was metamorphosed during the late stages of the Variscan orogeny (Late Paleozoic; ~320–260 Ma), while Biševac et al. (2010), using Kübler & Árkai indices accompanied by K-Ar dating of illite-muscovite rich fractions, found evidence for Cretaceous very low- to low-grade overprint (~100–80 Ma). The lower and middle parts of the RC are intruded by metabasic rocks which, according to Pamić & Jamičić (1986) show clear signs of metamorphic alteration with plagioclase metamorphosed into clinozoisite and sericite accompanied by newly formed sodic plagioclase, while clinopyroxene is moderately to strongly altered to fine-grained aggregate of chlorite, uralite and epidote. Based on the field relations the RC unconformably overlies the PsC (Jamičić 1983, 1988) and contains a Westphalian microflora (Brkić et al. 1974) which documents a Pennsylvanian age of the protolith. Since the Westphalian microflora was found in the middle pocket of the RC, Pamić & Jamičić (1986) presumed that the higher parts of the complex belong to the Lower Permian and deeper parts probably to the Upper Devonian. Furthermore, the K-Ar dating on clinopyroxene monomineralic concentrate from ophitic metagabbro, which intruded the RC (Pamić & Jamičić 1986), gave ages of 416.0±9.0 and 318.6±12.2 Ma (Pamić et al. 1988; Pamić & Lanphere 1991) which are partly consistent with paleofloristic determinations. The K-Ar age determinations on two slates from Paleozoic complexes yielded K-Ar whole-rock ages of 203.9±6.9 Ma and 100.6±3.5 Ma, which, according to Pamić et al. (1988), apparently represent partially or completely reset ages, due to subsequent heating. Jamičić (1988) proposed a model, based on paleofloristic and structural data, in which the metasedimentary rocks of the Radlovac Complex are considered to represent the detritus of the surrounding igneous and metamorphic rocks of the local pre-Variscan and Variscan crust (PsC and PaC Complexes, respectively). While RC transgressively overlay the PsC from one side, it is in tectonic contact with PaC from the other (Fig. 1). The geological evolution of the surrounding rocks is also quite complex and interesting. The PsC is assumed to be formed by a metamorphic event during the Baikalian orogeny (Late Precambrian to Early Paleozoic) and overprinted and retrogressed by younger metamorphic events (Jamičić 1988). It contains green schist to amphibolite facies rocks occurring in association with metabasites. The K-Ar ages on hornblende monomineralic concentrate from amphibolites yielded Variscan ages ranging from 376.4±11.5–352.6±8.5 Ma (Pamić et al. 1988; Pamić 1998). These metamorphic rocks are intruded by small bodies of I-type granites of Variscan age ranging from 423.7±12.9 to 336.3±8.4 Ma based on the K-Ar dating of muscovite (Pamić et al. 1988, 1996; Pamić & Lanphere 1991). The PaC endured, according to Jamičić (1988), metamorphism and migmatitization during the Caledonian orogeny (Ordovician to Early Devonian; ~490–390 Ma). It consists predominantly of S-type granites joined by migmatites and migmatitic gneisses of Variscan age (K-Ar ages of biotite and muscovite fall between 272.2±6.4–336.3±8.4 Ma; Pamić et al. 1988), which grade into amphibolite facies sequences composed of garnetiferous amphibolites, paragneisses and mica-schists (Pamić 1986; Pamić & Lanphere 1991).

Regarding the metamorphic evolution of the Slavonian Mountains, there is a general agreement about medium- to high-grade pre-Variscan and Variscan metamorphism (Balen et al. 2006; Horvath et al. 2010). Some authors attributed a great role to a late Variscan low-grade metamorphic event (Jamičić 1988), while new studies (Biševac et al. 2010, 2011) show the existence of Cretaceous low-T regional metamorphism in the area.

Analytical methods

Research on representative metasedimentary rock samples sampled in several quarries and profiles along the roads and rivers involved thin section and heavy mineral slide analyses

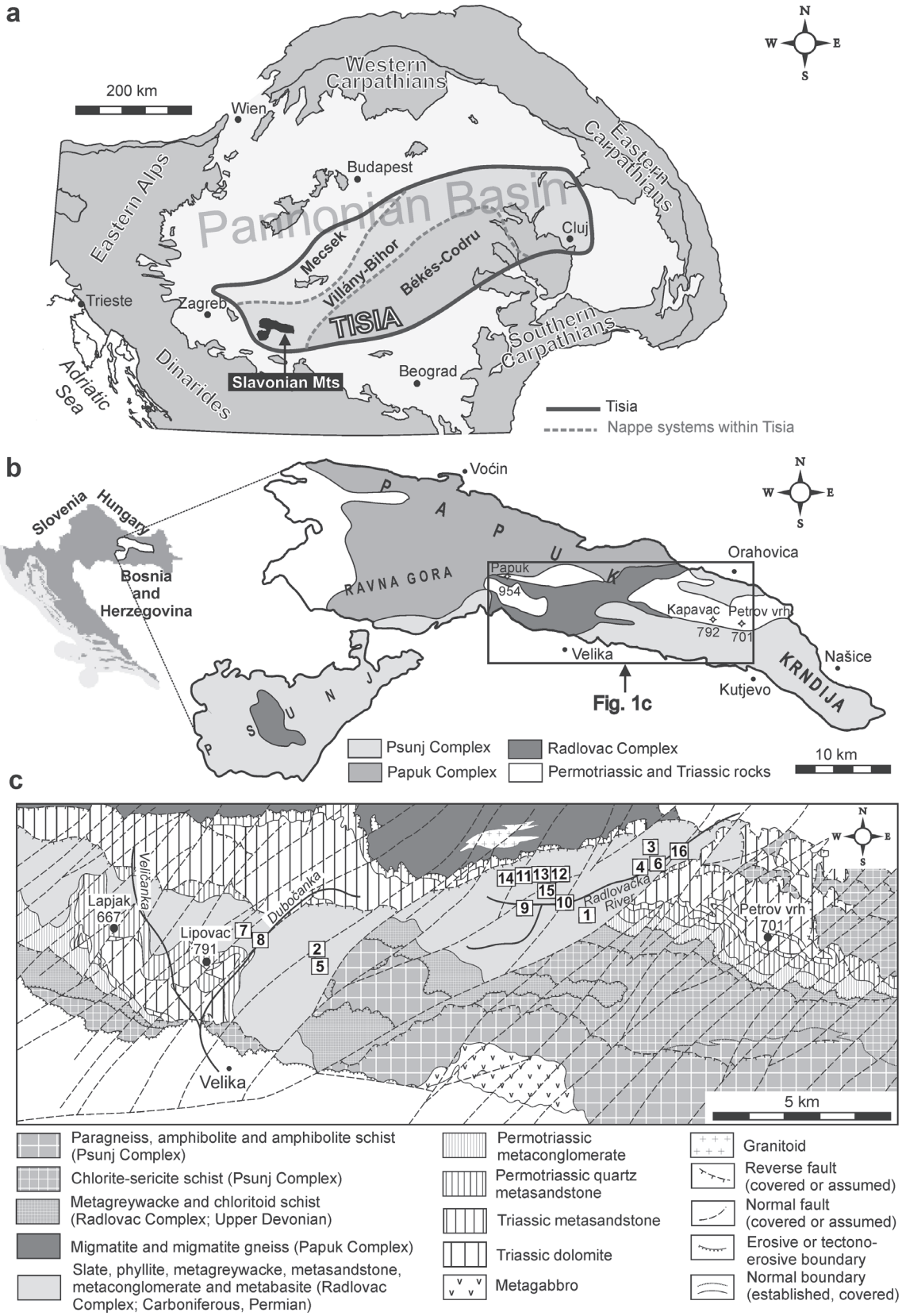

Fig. 1. a — Tectonic setting of the Tisia Unit within the Alpine-Carpathian-Dinaric framework with the position of the Slavonian Mts and **b** — sketch map of Slavonian Mts (Papuk, Psunj, Ravna gore and Krndija) with defined complexes after Jamičić (1988) and approximate position of the studied area (marked by the black box). **c** — Simplified geological map (Jamičić & Brkić 1987) of the investigated area showing the position of the samples within the Radlovac Complex.

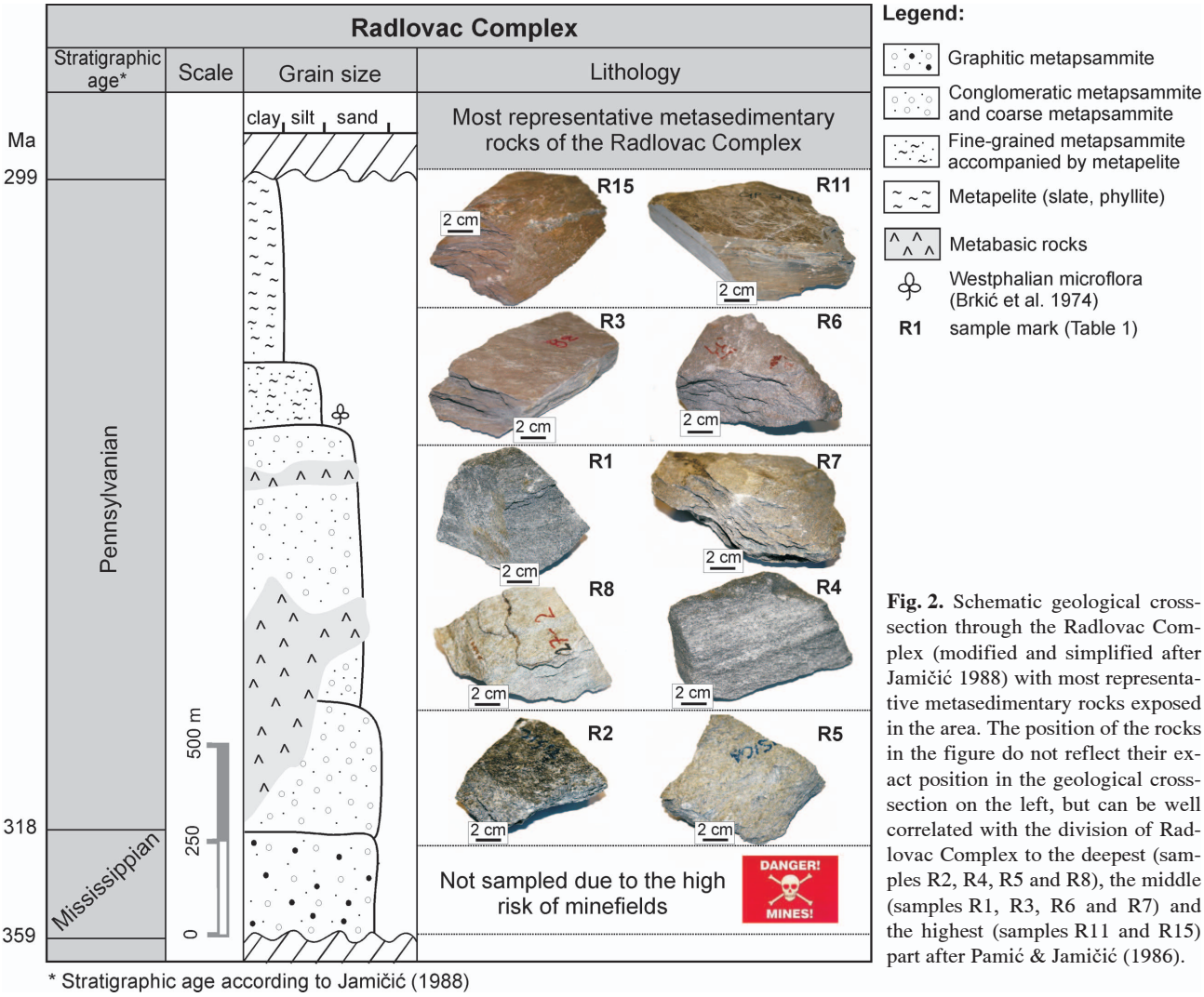

Fig. 2. Schematic geological cross-section through the Radlovac Complex (modified and simplified after Jamičić 1988) with most representative metasedimentary rocks exposed in the area. The position of the rocks in the figure do not reflect their exact position in the geological cross-section on the left, but can be well correlated with the division of Radlovac Complex to the deepest (samples R2, R4, R5 and R8), the middle (samples R1, R3, R6 and R7) and the highest (samples R11 and R15) part after Pamić & Jamičić (1986).

with a polarizing microscope, mineral chemical composition analyses and age dating by electron microprobe and geochemical whole-rock analyses.

Whole-rock analyses were performed in ACME Analytical Laboratories Ltd., Vancouver (Canada). Following a lithium metaborate/tetraborate fusion and dilute nitric digestion, trace elements were determined by ICP–MS, and major elements by ICP-ES. The analytical accuracy was controlled using geological standard materials and is estimated to be within a 1 % error (1σ, relative) for most major elements (exception: ±3 % for P_2O_5), and within a ±15 % error range (1σ, relative) for the trace elements (incl. REEs), for values greater than 10 times the detection limit.

Mineral analyses were carried out on a JEOL JX8600 microprobe housed at Salzburg University. A particular emphasis was placed on the analysis of accessory monazite and xenotime in order to estimate formation ages by means of the Th-U-total Pb method (Suzuki et al. 1991; Montel et al. 1996). Monazite and xenotime were analysed following the routine of Krenn et al. (2008). Single monazite ages and errors were calculated after Montel et al. (1996), weighted average ages with the software Isoplot 2.49e (Ludwig 2001). Isochron age was calculated using the least-squares fitting method of York (1966).

Whole-rock powder XRD analyses of samples (a semiquantitative mineral composition) were performed on a Philips X'Pert Pro diffractometer equipped with a X'celerator detector using CuK_α radiation from a tube operating at 40 kV and 45 mA at Department of Geology, Faculty of Science, University of Zagreb. The step width was 0.017° 2Θ with 43 s counting time per step; the samples were run between 4 and 65° 2Θ.

For quantitative heavy mineral analyses metapsammites were first crushed in a jaw crusher. The heavy minerals were extracted from the 63–125 μm sieve fraction by gravity separation in $CHBr_3$ (2.87 g/cm^3) and mounted on glass slides. Proportions of heavy mineral species were obtained by ribbon-counting (Mange & Maurer 1991) of approximately 300 non-opaque, non-micaceous grains in each representative sample using a polarizing microscope.

For the separation of zircons from rock powder samples (fraction of 250–125 μm) a wet vibrating table was used. Heavy mineral fraction was collected by pipette, dried in dryer at 50 °C and then separated by a permanent magnet and by magnetic separator. From the non-magnetic fraction, zircon

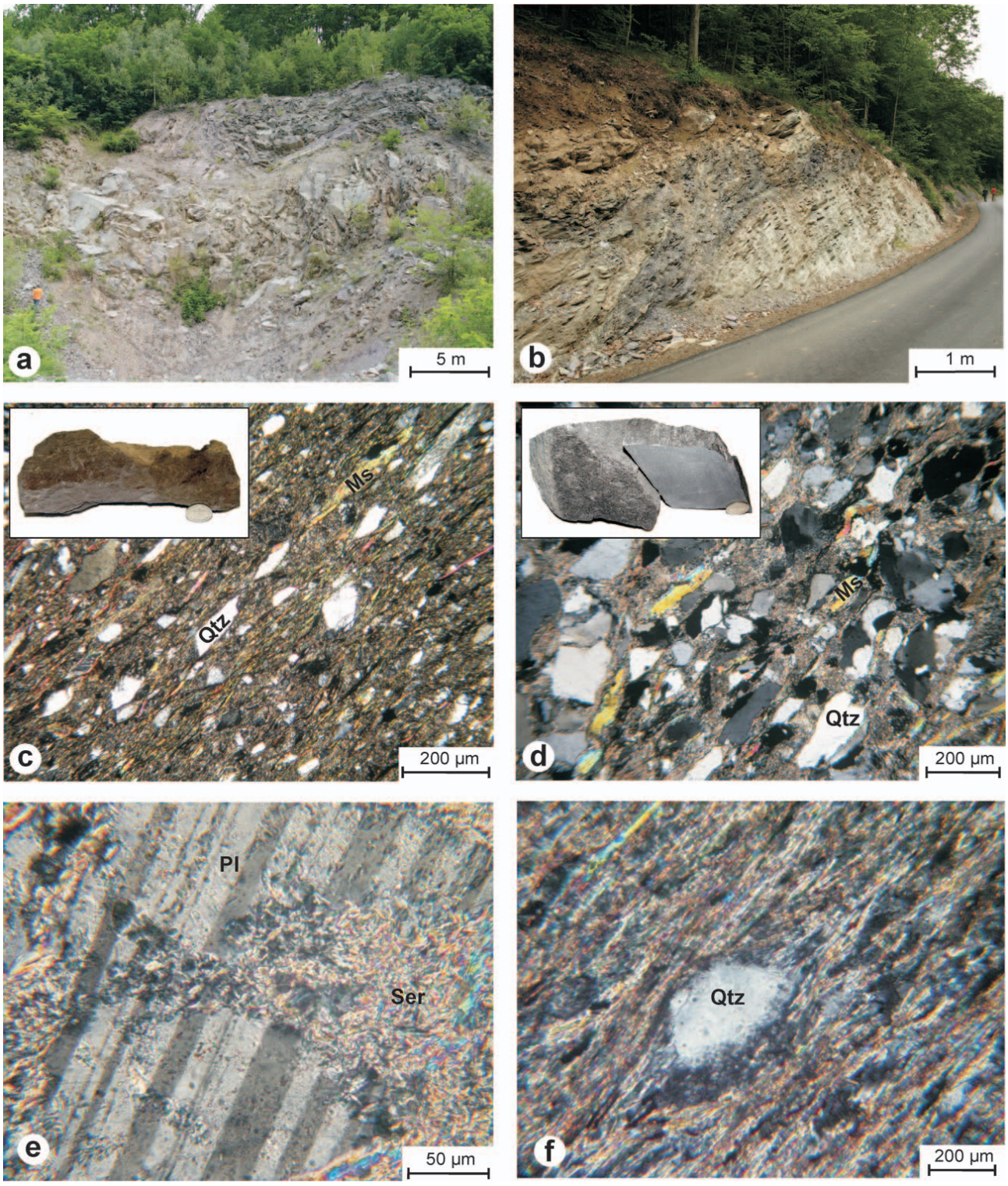

Fig. 3. Macro- and microphotographs (cross-polarized light) showing field relations and some characteristic microstructural features of the Radlovac Complex metasedimentary rocks. **a** — Radlovac quarry near Radlovačka River in the north-east part of the complex. **b** — Radlovac Complex metasedimentary rocks along the road near Tisica quarry in the central part of the complex. **c** — Typical metapelite (phyllite) sample (R9) showing continuous cleavage and foliation defined by fine-grained micaceous material and elongated quartz grains. **d** — Characteristic schistose metapsammite (R1) showing well developed foliation defined by subparallel muscovite and quartz grains embedded in fine-grained matrix of sericite, chlorite and recrystallized quartz. **e** — Alteration in sample R1 typical for metasedimentary rocks of the Radlovac Complex (sericitization). **f** — Syndeformational growth of sericite strain fringes in the pressure shadows of detrital quartz grain (sample R14).

grains were separated manually by hand-picking using binocular lens. Zircon photographs used for zircon typology study were obtained by TESCAN scanning electron microscope equipped with back-scatter electron detector and operated at 20 kV at the Department of Geology, Faculty of Science, University of Zagreb. The zircons were carbon coated.

Results

Petrography

Metasedimentary rocks of the Radlovac Complex are well exposed in several quarries and road-cuts along the Radlovačka River (Fig. 1) in the central part of the complex going from SW to NE (Fig. 3a) and along the road north of the town of Velika (Fig. 3b). The most common metasedimentary rocks of the RC are fine-grained metapelites and moderately sorted metapsammites. Here, the term metapelite stands for metasedimentary rock containing >70 % fine-grained matrix, while the term metapsammite is used for metasedimentary rocks containing <40 % of matrix. Both groups have similar mineral composition with dominant quartz, illite-muscovite, chlorite and plagioclase, subordinate K-feldspar, paragonite and hematite and rare carbonate minerals (Table 1). Reddish, green and grey coloured metapelites are characterized by typical microlepidoblastic texture, while characteristic spaced cleavage is defined by elongated quartz grains (20–50 μm), detrital muscovite flakes and dominant fine-grained micaceous-chlorite mixture (Fig. 3c). Typical metapsammites show schistosity marked by subparallel muscovite flakes and elongated quartz grains with apparent grain sizes of 50–300 μm, and comprising subordinate plagioclase embedded in clay- to silt-sized matrix of recrystallized quartz, illite-muscovite and chlorite, and in some samples paragonite (Fig. 3d). Since the matrix content for all samples is relatively high and signs of mineralogical alteration are evident, modal composition of the samples was not determined. Signs of alteration of feldspars to clay minerals occur in all samples (Fig. 3e). Other alterations include syndeformational growth of sericite/quartz strain fringes in the pressure shadows of detrital quartz (Fig. 3f) and plagioclase. This interesting feature indicates the percolation of K-rich fluids (Sutton et al. 1990; Frimmel 1994), a characteristic phenomenon for the green schist facies metasedimentary rocks (Bucher & Frey 1994).

The detrital heavy mineral assemblages of the studied Radlovac representative metapsammites are dominated by apatite and other minerals like zircon, tourmaline and rutile (Table 1). Other heavy minerals such as epidote/zoisite, monazite and titanite occur in trace amounts. Apatite occurs both as fresh and partially altered grains, mostly colourless, sometimes with a brownish core. Grains are usually irregular in shape or stubby prisms. Zircons mostly occur as irregular and fragmented grains, translucent to yellowish or brownish in colour. Euhedral grains are also commonly encountered. Tourmaline grains are dominantly irregular in shape and pervasively display green-brown to yellowish pleochroic colours, although the prismatic crystals can be observed. Authigenic tourmaline is sporadically encountered as overgrowths. Monazite is discussed in a separate chapter.

Monazite age dating

Monazite was studied in the metapsammite samples R1 and in the metapelite sample R15 which served as two representative samples from the Radlovac Complex. Monazite from sample R1 is ca. 20–50 μm large (Fig. 4), sub-anhedral and occurs in the matrix as well as inclusions in coarse muscovite and quartz. The grain boundaries are irregular and partly resorbed. The chemical Th-U-Pb dates of single monazite analyses are listed in Table 2. Analyses from both core and rim domains exclusively provide Variscan ages, which combined

Table 1: Semiquantitative mineral composition of the Radlovac Complex metasedimentary rocks together with heavy mineral data of the representative metapsammites.

Radlovac Complex metasedimentary rocks																
	Metapsammites								Metapelites							
Sample	**R1**	**R2**	**R3**	**R4**	**R5**	**R6**	**R7**	**R8**	**R9**	**R10**	**R11**	**R12**	**R13**	**R14**	**R15**	**R16**
Lithology	**Msn**	**CMgr**	**Mgr**	**Msn**	**CMgr**	**Mgr**	**Msn**	**Msn**	**Phy**	**Slt**	**Phy**	**Phy**	**Phy**	**Phy**	**Slt**	**Slt**
Mineral composition																
Quartz	■■	■■	■■	■■	■■	■■	■■	■■	■	■	■	□	■	□	■	■
Illite-muscovite	■	■■	■	■	■	■	■	□	■■	■■	■■	■■	■■	■■	■■	■■
Plagioclase	□	□	□	□	■	□	□	□	x	□	□	□	□	□	x	□
K-feldspar	–	–	–	–	–	–	x	–	–	–	–	–	–	x	–	–
Chlorite	□	□	□	□	x	□	□	□	□	□	□	□	□	□	x	□
Hematite	–	–	x	–	–	–	–	–	x	–	x	x	x	x	□	–
Paragonite	–	–	–	–	–	–	–	□	x	–	–	–	–	–	x	x
Calcite	–	–	–	–	–	–	–	–	–	x	–	–	–	–	–	–
Heavy minerals (%)																
Zircon	34				15		27	35								
Tourmaline	20				7		5	2								
Rutile	8				4		6	4								
Apatite	34				72		57	57								
Epidote/Zoisite	1				–	–	–	+								
Monazite	+				–		1	–								
Titanite	–				+		1	–								
Unindentified	3				2		3	2								

Msn — metasandstone
CMgr — conglomeratic metagreywacke
Mgr — metagreywacke
Phy — phyllite
Slt — slate
■■ — dominant; ■ — abundant; □ — significant; **x** — poor; + — present, but below 0.5 %; – — not present.

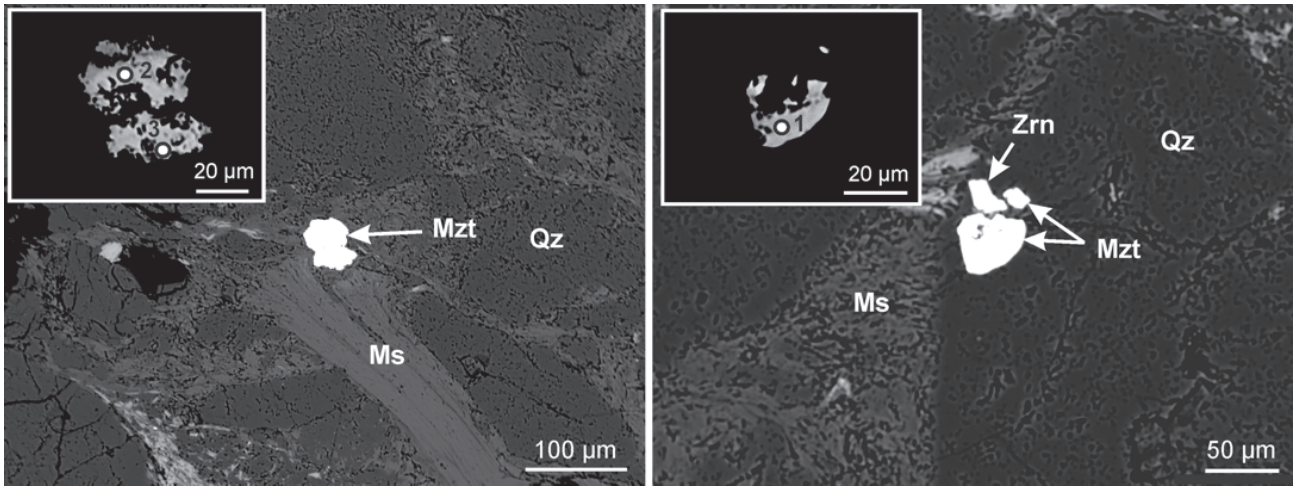

Fig. 4. Back-scattered electron (BSE) images of monazite in metapsammite sample R1. Numbers refer to analyses in Table 3. Mineral abbreviation after Whitney & Evans (2010). **Qz** — quartz, **Mzt** — monazite, **Zrn** — zircon, **Ms** — muscovite.

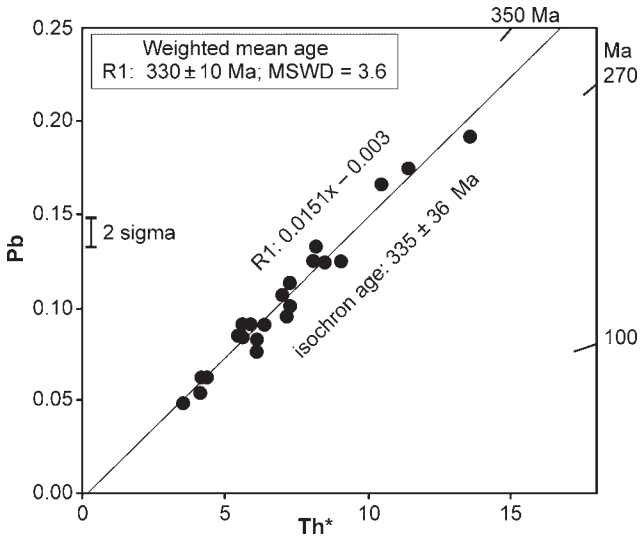

Fig. 5. Th* vs. Pb (wt. %) diagram after Suzuki et al. (1991) with monazite analyses from sample R1 and standard isochron calculated for Variscan monazite.

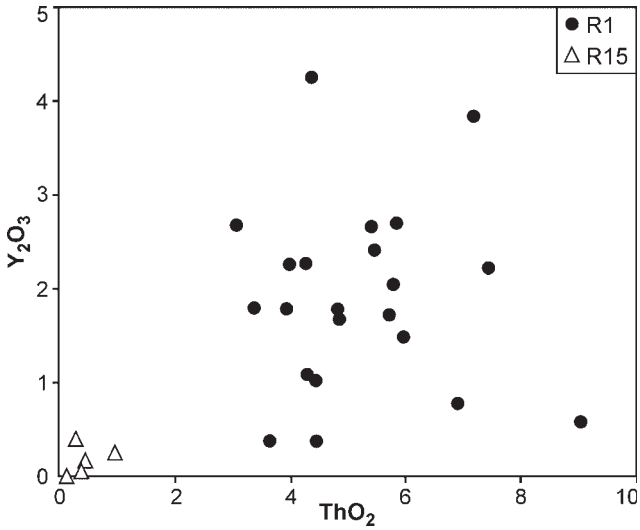

Fig. 6. Y_2O_3 vs. ThO_2 (wt. %) plot with monazite analyses for samples R1 and R15.

provide a weighted average age of 330 ± 10 Ma (95 % conf., MSWD: 3.6). Figure 5 shows that the data from sample R1 is arrange along the Th* vs. Pb isochron with a slope of 0.0151× ± 0.0017× (isochron age: 335 ± 36 Ma) and a Y-axis intersection value of –0.003. Monazite grains in sample R1 are characterized by moderate to high Th, U and Y contents (3–9 wt. % ThO_2, 0.2–2 wt. % UO_2, 1–4 wt. % Y_2O_3; Table 3; Fig. 6) and xenotime values ranging from ca. 1–10 mol %. According to the monazite-xenotime miscibility gap thermometers of Heinrich et al. (1997), Gratz & Heinrich (1997) and Pyle et al. (2001) maximum xenotime values of 10 mol % imply formation temperatures of 600–800 °C (Table 2; Fig. 7).

Compared to monazite grains from the sample R1, those from sample R15 are much smaller (< 10 μm) and have a much lower ThO_2 (< 1 wt. %) and Y_2O_3 (< 0.5 wt. %) (Table 3; Fig. 6). Due to the low concentration of Th, U and Pb they could not be used for dating by means of electron microprobe.

Xenotime geochemistry

Xenotime was detected in sample R1. Xenotime grains are small (< 20 μm) and practically always in association with zircon (Fig. 8). One type of xenotime (type 1) forms eu-subhedral, partially rounded shapes and shows a zonation in backscattered electron (BSE) imagery (Fig. 8a). The other type of xenotime (type 2), characterized by resorbed and/or dissolved boundaries, occurs as overgrowths on detrital zircon grains (Fig. 8b) and occasionally as vein and fracture fill within zircon grains. These two xenotime types are also dis-

Table 2: Concentration (wt. %) and age data for monazite and xenotime from samples R1 and R15 calculated after Montel et al. (1996). Th* values are after Suzuki et al. (1991). Formation temperatures of monazite calculated after Pyle et al. (2001), Heinrich et al. (1997) and Gratz & Heinrich (1997) are also shown. ** — possible contamination due to the small grain size.

										Formation temperature (°C)		
Sample	**Position**	**Matrix**	**Th (wt. %)**	**U (wt. %)**	**Pb (wt. %)**	**Th* (wt. %)**	**Age**	**± 2σ (Ma)**	**X(Xtm)**	**Pyle et al. (2001)**	**Heinrich et al. (1997)**	**Gratz & Heinrich (1997)**
Monazite												
R1 Mzt1-2	rim	Qz–Ms	3.510	1.123	0.095	7.153	298	22	0.09	584	674	675
R1 Mtz1-3	core	Qz–Ms	3.447	0.750	0.090	5.887	345	27	0.07	518	614	579
R1 Mzt2	core	Ms	5.085	0.310	0.083	6.092	304	26	0.08	561	653	642
R1 Mzt3	core	Qz–Ms	5.017	0.333	0.076	6.094	281	26	0.07	535	629	603
R1 Mzt4	rim	Qz–Ms	3.739	0.573	0.084	5.602	335	28	0.08	555	647	632
R1 Mzt5	rim	Qz	4.741	0.783	0.113	7.288	347	22	0.09	601	689	700
R1 Mzt6	rim	Ab–Qz	2.973	0.363	0.054	4.149	291	38	0.07	521	617	584
R1 Mzt7	core	Qz	7.950	0.158	0.124	8.465	327	19	0.05	408	515	418
R1 Mzt7	rim	Ms	3.219	0.103	0.049	3.554	307	45	0.03	220	344	141
R1 Mzt8	core	Qz	5.241	1.173	0.125	9.047	309	25	0.06	463	565	498
R1 Mzt9	core	Qz–Ms	6.313	1.559	0.174	11.387	343	20	0.12	669	751	801
R1 Mzt10	rim	Ms	3.935	0.518	0.091	5.623	361	28	0.03	222	346	145
R1 Mzt11	core	Qz	6.541	2.164	0.192	13.572	318	17	0.07	520	616	582
R1 Mzt12	core	Qz	2.695	0.845	0.084	5.446	347	29	0.09	589	679	683
R1 Mzt13	rim	Ms	4.257	1.168	0.125	8.061	348	20	0.06	494	592	543
R1 Mzt14	core	Qz	5.124	0.662	0.100	7.274	309	22	0.08	573	664	659
R1 Mzt15	rim	Qz–Ms	6.076	1.339	0.166	10.440	357	21	0.03	301	418	261
R1 Mzt16	rim	Qz–Ms	4.243	1.202	0.133	8.160	365	19	0.07	518	614	578
R1 Mzt17	rim	Ms	4.793	0.673	0.107	6.985	343	23	0.08	569	661	654
R1 Mzt18	core	Qz	3.906	0.131	0.062	4.332	321	37	0.05	440	543	464
R1 Mzt18	rim	Qz	3.779	0.121	0.062	4.174	332	38	0.06	451	553	480
R1 Mzt19	rim	Qz	3.847	0.779	0.091	6.377	320	25	0.13	697	776	841
**R15 Mzt1	small	Ab–Qz	0.837	0.031	0.020	0.940	–	–	0.02	184	312	89
**R15 Mzt2	small	Qz	0.330	0.081	0.027	0.607	–	–	0.02	61	200	–92
**R15 Mzt3	small	Ms	0.399	0.027	0.017	0.491	–	–	0.02	160	290	53
**R15 Mzt4	small	Qz–Ms	0.120	0.109	0.017	0.489	–	–	0.01	–73	78	–289
Xenotime												
R1 Xtm1	core	Qz	0.172	0.586	0.048	2.103	–	–	–	–	–	–
R1 Xtm2	core	Qz	0.471	2.403	0.116	8.276	317	27	–	–	–	–
R1 Xtm3	core	Zrn	0.130	0.234	0.053	0.950	–	–	–	–	–	–
R1 Xtm4	core	Qz	0.482	2.816	0.127	9.616	298	23	–	–	–	–
R1 Xtm5	core	Zrn	0.144	0.213	0.023	0.852	–	–	–	–	–	–
R1 Xtm6	core	Qz	0.492	2.622	0.115	8.989	288	25	–	–	–	–
R1 Xtm7	core	Zrn	0.108	0.181	0.030	0.724	–	–	–	–	–	–
R1 Xtm8	core	Zrn	0.103	0.160	0.023	0.644	–	–	–	–	–	–

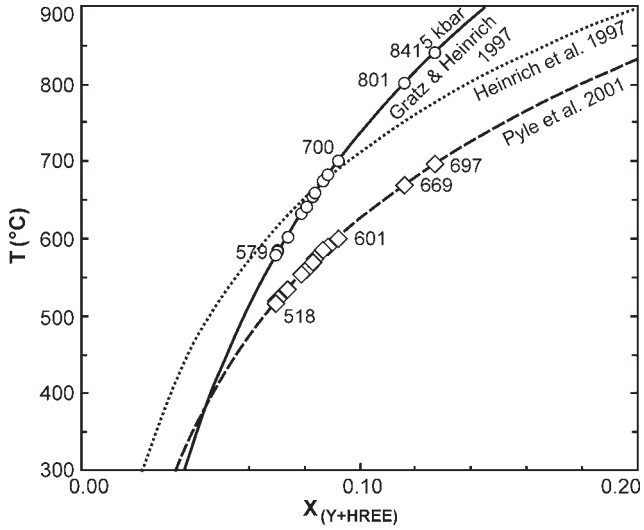

Fig. 7. Monazite formation temperature according to thermometers of Gratz & Heinrich (1997), Heinrich et al. (1997) and Pyle et al. (2001).

criminated according to their chemistry. Type 1 xenotime is characterized by higher U and Th (0.66–3.19 wt. % and 0.2–0.56 wt. %, respectively) compared to type 2 xenotime (0.18–0.26 wt. % and 0.12–0.16 wt. %, respectively) (Fig. 9a). Additionally, type 1 xenotime has lower Eu_2O_3 (up to 0.12 wt. %), Dy_2O_3 (2.63–4.22 wt. %) and Gd_2O_3 (3.73–4.71 wt. %) and higher Yb_2O_3 (2.97–5.46 wt. %) compared to Eu_2O_3 (0.93–1.11 wt. %), Dy_2O_3 (4.90–5.06 wt. %) and Gd_2O_3 (8.71–9.32 wt. %) and Yb_2O_3 (1.31–1.37 wt. %) characteristic for type 2 xenotime (Table 4; Fig. 9b and c).

Whole-rock geochemistry

The whole-rock element composition of the studied metasediments is presented in Appendix. Metapsammites have higher average SiO_2 and lower Al_2O_3, Fe_2O_3, MgO, Na_2O and K_2O (Appendix) compared to metapelites which correlates with the dominance of quartz in the metapsammites and that of clay minerals and hematite in metapelites (Table 1). Metapsammites can be characterized by a felsic bulk composition with ca. 61–77 wt. % SiO_2, 10–18 wt. % Al_2O_3,

Table 3: Selected electron microprobe analyses (wt. %) of monazite from samples R1 and R15.

Sample	R1	R1	R1	R1	R1	R1	R1	R1	R1	R1	R15	R15
Position	Mzt1-2 rim	Mtz1-3 core	Mzt2 core	Mzt3 core	Mzt7 core	Mzt7 rim	Mzt9 core	Mzt15 rim	Mzt18 core	Mzt18 rim	** Mzt1 core	** Mzt3 core
Matrix	Qz–Ms Fig. 4-2	Qz–Ms Fig. 4-3	Ms	Qz–Ms	Qz	Ms	Qz–Ms Fig. 4-1	Qz–Ms	Qz	Qz	Ms	Qz–Ms
SiO_2	0.25	0.35	0.38	0.41	1.89	0.65	0.42	0.46	0.51	0.53	1.38	0.97
P_2O_5	29.24	30.15	28.70	29.14	26.94	28.55	29.08	29.06	29.16	28.86	27.76	29.40
CaO	0.93	0.79	0.87	0.91	0.20	0.11	1.47	1.30	0.52	0.47	2.43	2.61
Y_2O_3	2.25	1.78	2.04	1.73	0.57	0.38	3.85	0.79	1.04	1.09	0.05	0.16
La_2O_3	12.66	11.92	9.65	8.35	11.96	13.86	11.04	13.14	12.51	11.95	13.47	12.91
Ce_2O_3	29.37	29.45	27.97	28.15	29.94	34.00	27.22	29.91	30.77	30.87	31.78	31.49
Pr_2O_3	3.16	3.15	3.15	3.50	3.24	3.63	2.79	2.96	3.41	3.49	3.16	3.20
Nd_2O_3	12.37	12.64	14.01	14.27	10.63	11.29	11.47	11.40	12.43	12.22	11.36	12.33
Sm_2O_3	2.27	2.19	3.42	3.73	2.91	2.75	2.22	1.99	2.59	2.58	1.85	1.90
Gd_2O_3	2.29	1.98	2.27	2.27	1.68	1.23	1.75	1.12	1.94	1.92	0.85	1.15
Dy_2O_3	0.69	0.53	0.45	0.47	0.31	0.12	0.86	0.16	0.46	0.51	0.18	0.15
Er_2O_3	0.14	0.09	0.08	0.09	0.05	0.01	0.08	0.05	0.06	0.07	0.01	0.04
ThO_2	3.99	3.92	5.79	5.71	9.05	3.66	7.18	6.91	4.44	4.30	0.38	0.45
UO_2	1.27	0.85	0.35	0.38	0.18	0.12	1.77	1.52	0.15	0.14	0.09	0.03
PbO	0.10	0.10	0.09	0.08	0.14	0.05	0.19	0.18	0.07	0.07	0.03	0.02
Total	101.00	99.88	99.23	99.17	99.68	100.42	101.45	100.95	100.08	99.07	94.77	96.80
a.p.f.u. based on 4 oxygens												
Si	0.01	0.01	0.02	0.02	0.08	0.03	0.02	0.02	0.02	0.02	0.05	0.04
P	0.97	0.99	0.97	0.98	0.92	0.96	0.96	0.97	0.97	0.98	0.90	0.93
Ca	0.04	0.03	0.04	0.04	0.01	0.00	0.06	0.06	0.02	0.02	0.10	0.10
Y	0.05	0.04	0.04	0.04	0.01	0.01	0.08	0.02	0.02	0.02	0.00	0.00
La	0.18	0.17	0.14	0.12	0.18	0.20	0.16	0.19	0.18	0.18	0.19	0.18
Ce	0.42	0.42	0.41	0.41	0.44	0.50	0.39	0.43	0.44	0.45	0.44	0.43
Pr	0.05	0.04	0.05	0.05	0.05	0.05	0.04	0.04	0.05	0.05	0.04	0.04
Nd	0.17	0.18	0.20	0.20	0.15	0.16	0.16	0.16	0.18	0.17	0.16	0.17
Sm	0.03	0.03	0.05	0.05	0.04	0.04	0.03	0.03	0.04	0.04	0.02	0.02
Gd	0.03	0.03	0.03	0.03	0.02	0.02	0.02	0.01	0.03	0.03	0.01	0.01
Dy	0.01	0.01	0.01	0.01	0.00	0.00	0.01	0.00	0.01	0.01	0.00	0.00
Er	0.00	0.00	0.00	0.00	0.00	0.00	0.00	0.00	0.00	0.00	0.00	0.00
Th	0.04	0.03	0.05	0.05	0.08	0.03	0.06	0.06	0.04	0.04	0.00	0.00
U	0.01	0.01	0.00	0.00	0.00	0.00	0.02	0.01	0.00	0.00	0.00	0.00
Pb	0.00	0.00	0.00	0.00	0.00	0.00	0.00	0.00	0.00	0.00	0.00	0.00
Tetr.	0.98	1.01	0.99	1.00	1.00	0.99	0.98	0.99	0.99	1.00	1.01	1.01
A[9]	1.03	0.99	1.02	1.00	1.00	1.02	1.04	1.02	1.01	1.01	1.01	1.01

** — possible contamination due to the small grain size; Tetr. = Si + P; A[9] = ΣREE + Th + U + Pb + Ca + Y

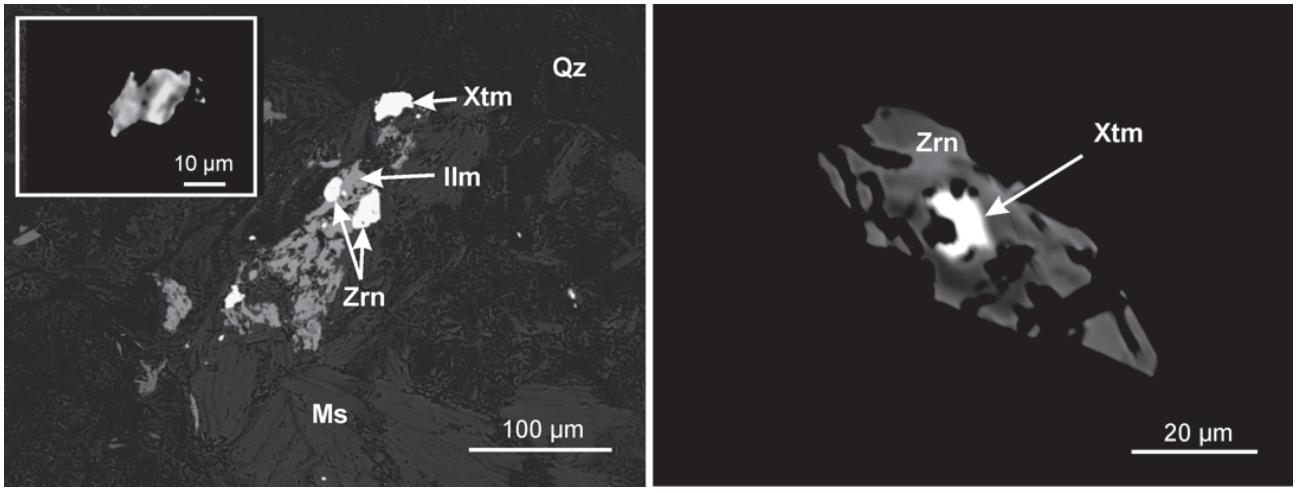

Fig. 8. Back-scattered electron (BSE) images of xenotime in metapsammite sample R1. **a** — Igneous-detrital xenotime showing brighter and darker domains. **b** — Hydrothermal xenotime occurring as overgrowth on detrital zircon grain. Mineral abbreviations after Whitney & Evans (2010). **Qz** — quartz, **Xtm** —xenotime, **Zrn** — zircon, **Ms** — muscovite, **Ilm** — ilmenite.

Table 4: Electron microprobe analyses (wt. %) of xenotime from sample R1.

Sample	R1 Xtm1	R1 Xtm2	R1 Xtm3	R1 Xtm4	R1 Xtm5	R1 Xtm6	R1 Xtm7	R1 Xtm8
Position	core	core	core	core	core	core	core	core
Matrix	Qz	Qz	Zrn	Qz	Zrn	Qz	Zrn	Zrn
Origin	Igneous-detrital	Igneous-detrital	Hydrothermal	Igneous-detrital	Hydrothermal	Igneous-detrital	Hydrothermal	Hydrothermal
SiO_2	0.02	0.71	0.11	0.77	0.14	0.64	0.10	0.17
Al_2O_3	0.00	0.00	0.24	0.11	0.23	0.00	0.04	0.08
P_2O_5	35.67	35.33	35.52	34.04	35.42	35.23	34.76	34.57
CaO	0.06	0.03	0.08	0.02	0.13	0.02	0.13	0.14
Y_2O_3	45.34	42.49	42.01	42.14	42.84	43.24	43.76	43.58
La_2O_3	0.01	0.09	0.00	0.00	0.05	0.10	0.11	0.10
Ce_2O_3	0.18	0.12	0.14	0.10	0.10	0.00	0.16	0.10
Pr_2O_3	0.21	0.00	0.01	0.21	0.09	0.09	0.16	0.08
Nd_2O_3	0.55	0.21	0.53	0.23	0.52	0.28	0.63	0.68
Sm_2O_3	0.52	0.40	1.48	0.41	1.38	0.24	1.48	1.53
Eu_2O_3	0.00	0.12	0.93	0.00	0.95	0.00	1.11	0.98
Gd_2O_3	4.71	3.88	8.89	3.73	9.11	3.75	8.71	9.32
Dy_2O_3	4.22	2.71	4.90	2.69	4.92	2.63	5.07	5.06
Er_2O_3	3.30	4.18	2.44	4.31	2.42	4.45	2.28	2.45
Yb_2O3	2.97	5.01	1.31	5.46	1.33	5.40	1.37	1.34
ThO_2	0.20	0.54	0.15	0.55	0.16	0.56	0.12	0.12
UO_2	0.66	2.73	0.26	3.19	0.24	2.97	0.20	0.18
PbO	0.04	0.12	0.06	0.13	0.03	0.10	0.03	0.03
Total	98.66	98.67	99.06	98.13	100.09	99.72	100.26	100.58
a.p.f.u. based on 4 oxygens								
Si	0.001	0.024	0.004	0.026	0.005	0.021	0.003	0.006
P	1.004	1.000	1.004	0.982	0.995	0.994	0.985	0.979
Al	0.000	0.000	0.009	0.004	0.009	0.000	0.002	0.003
Ca	0.002	0.001	0.003	0.001	0.004	0.001	0.005	0.005
Y	0.802	0.756	0.746	0.764	0.757	0.767	0.779	0.776
La	0.000	0.001	0.000	0.000	0.001	0.001	0.001	0.001
Ce	0.002	0.001	0.002	0.001	0.001	0.000	0.002	0.001
Pr	0.002	0.000	0.000	0.003	0.001	0.001	0.002	0.001
Nd	0.007	0.003	0.006	0.003	0.006	0.003	0.007	0.008
Sm	0.006	0.005	0.017	0.005	0.016	0.003	0.017	0.018
Gd	0.052	0.043	0.098	0.042	0.100	0.041	0.097	0.103
Eu	0.000	0.001	0.011	0.000	0.011	0.000	0.013	0.011
Dy	0.045	0.029	0.053	0.030	0.053	0.028	0.055	0.055
Er	0.034	0.044	0.026	0.046	0.025	0.047	0.024	0.026
Yb	0.030	0.051	0.013	0.057	0.013	0.055	0.014	0.014
Th	0.001	0.004	0.001	0.004	0.001	0.004	0.001	0.001
U	0.005	0.020	0.002	0.024	0.002	0.022	0.002	0.001
Pb	0.000	0.001	0.001	0.001	0.000	0.001	0.000	0.000
Tetr.	1.005	1.024	1.008	1.009	1.001	1.015	0.989	0.987
A[9]	0.990	0.961	0.988	0.985	1.001	0.974	1.020	1.024

Tetr. = Si + P; A[9] = ΣREE + Th + U + Pb + Ca + Y

1–6 wt. % Fe_2O_3 (Appendix) while metapelites contain ca. 49–62 wt. % SiO_2, 15–27 wt. % Al_2O_3 and 6–7 wt. % Fe_2O_3 (Appendix). However, due to the varying clay fraction in metapsammites with up to 40 %, some of them overlap chemically with metapelites and show relatively high A/CNK (Appendix).

Zr/Sc and Hf/Sc ratios for metapsammites (12–39 and 0.3–1.2, respectively) are somewhat higher then those for metapelites (8–16 and 0.2–0.5, respectively) (Appendix). The discrimination scheme of Roser & Korsch (1988) based on major elements shown in Fig. 10 indicate dominant input from primary felsic sources for metapelites, while metapsammites fall into the border of the recycled sources field and primary felsic source field (Fig. 10). The diagrams shown in Fig. 11, which are based on trace, relatively immobile, elements indicate dominant input of felsic igneous rocks for all samples.

Eu anomalies (Eu/Eu* = 0.6–0.8 for metapsammites; Eu/Eu* = 0.6–0.7 for metapelites) are present (Appendix). The values of provenance-indicative element ratios for both investigated groups of samples, such as Th/Sc, Th/Co and La/Sc (Appendix), are close or slightly above those for Upper Continental Crust (UCC), and according to Cullers (2000, 2002) and McLennan et al. (1993) indicate dominant felsic protolith source (Figs. 11 and 12).

The REE signatures of metapsammites and metapelites are similar and match those from the NASC (North American Shale Composite) and UCC (Fig. 13). The REE development of the surrounding older crystalline complexes, namely the Papuk Complex and the Psunj Complex (Fig. 13) can hardly be discriminated.

Zircon typology

Zircon grains from representative metapsammites (R1 and R2) were studied by means of zircon typology (Pupin 1980).

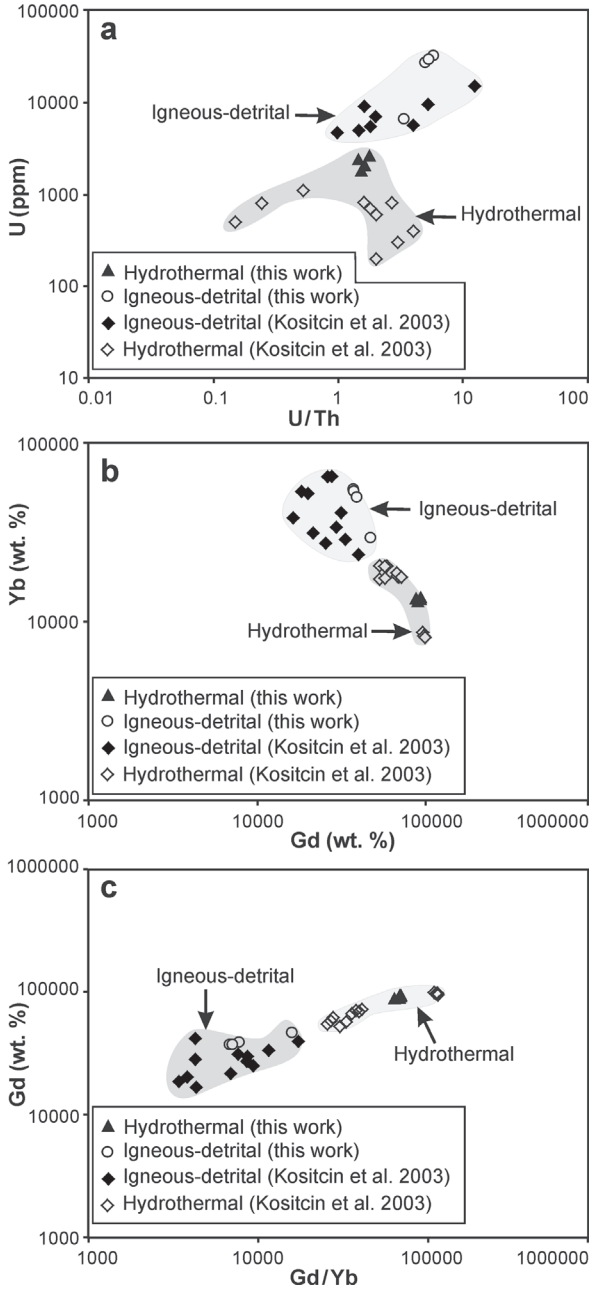

Fig. 9. Discrimination diagrams for igneous-detrital and hydrothermal xenotime. On each diagram data from Kositcin at al. (2003) are plotted as referent values for igneous-detrital and hydrothermal xenotime. **a** — Plot of U/Th against U (ppm) used for discrimination of xenotime types. **b** — The Gd vs. Yb (wt. %) discrimination diagram which separates hydrothermal xenotime from igneous-detrital xenotime. **c** — The Gd/Yb vs. Gd (wt. %) which clearly discriminates between igneous-detrital and hydrothermal xenotime.

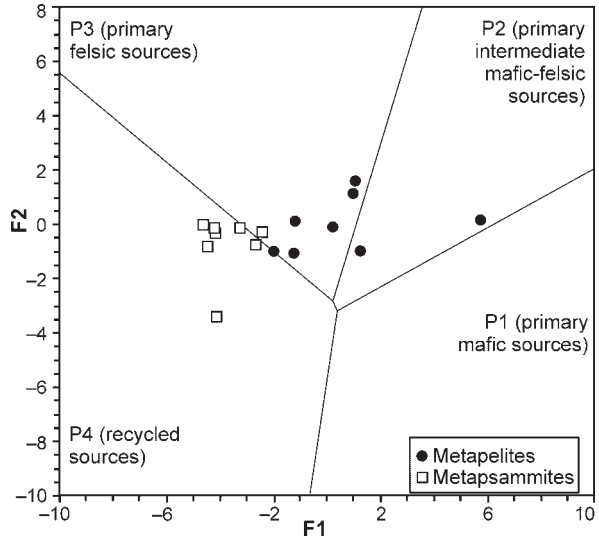

Fig. 10. Major element discrimination scheme for metasedimentary rocks of the Radlovac Complex irrespective of grain size, which takes major elements (Al, Fe, Mg, Ti, K, Na and Ca) into account. Diagram after Roser & Korsch (1988). **F1** — Discriminant function 1; **F2** — Discriminant function 2.

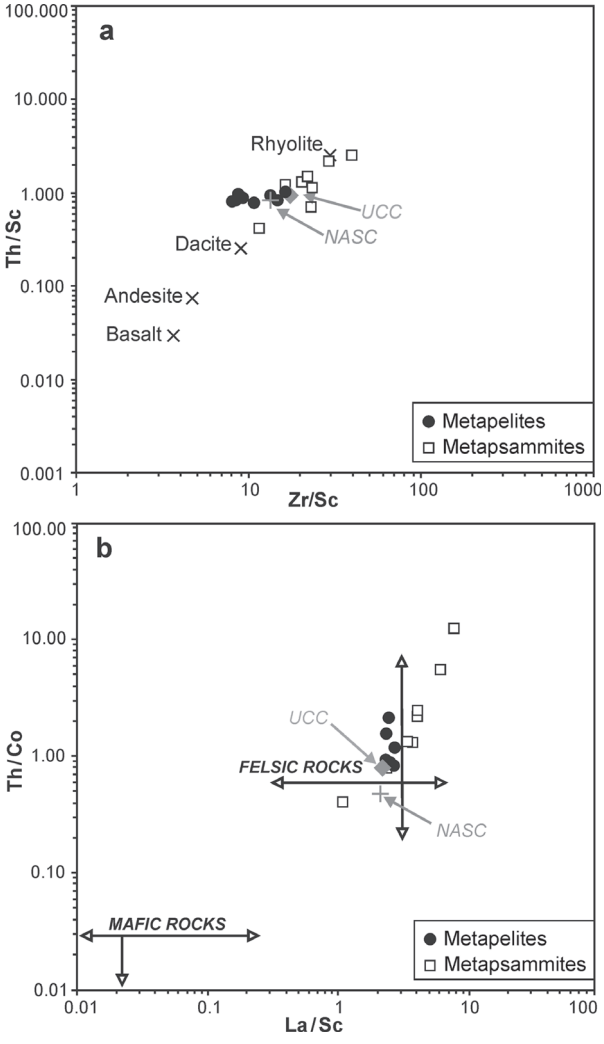

Fig. 11. a — Plot of Zr/Sc vs. Th/Sc showing a magmatic-arc trend (McLennan et al. 1993; Willan 2003). Plutonic equivalents plot in similar place. **b** — Plot of La/Sc vs. Th/Co after Cullers (2002). **UCC** — Upper Continental Crust (Taylor & McLennan 1985); **NASC** — North American Shale Composite (Gromet et al. 1984).

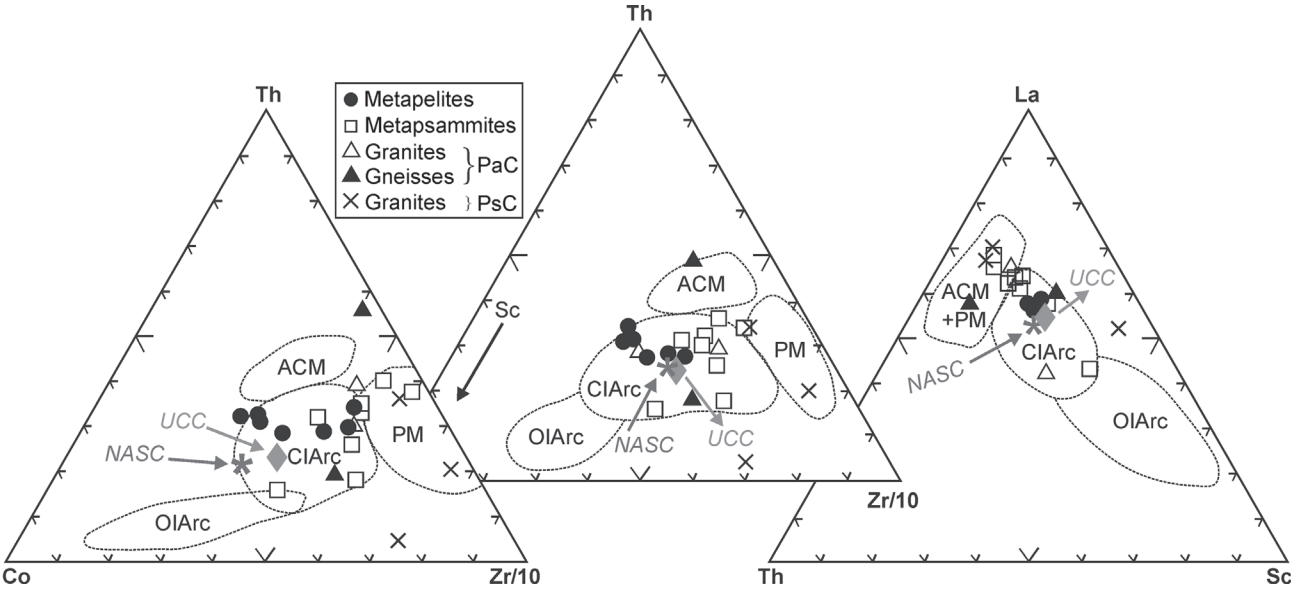

Fig. 12. Metasedimentary rocks from the Radlovac Complex together with referent rocks from the Papuk and Psunj Complexes in trace element diagrams with discrimination fields after Bathia & Crook (1986). **ACM** — active continental margin, **CIArc** — continental island arc, **OIArc** — oceanic island arc, **PM** — passive margin, **UCC** — Upper Continental Crust (Taylor & McLennan 1985), **NASC** — North American Shale Composite (Gromet et al. 1984).

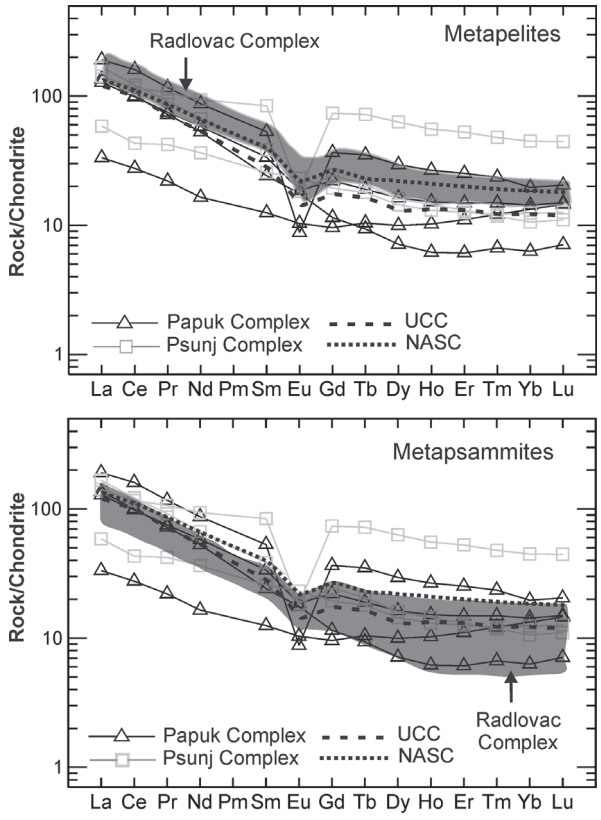

Fig. 13. Chondrite normalized REE patterns of the Radlovac Complex metasedimentary rocks. Characteristic rocks from the Papuk and Psunj Complexes, together with **UCC** — Upper Continental Crust (Taylor & McLennan 1985) and **NASC** — North American Shale Composite (Gromet et al. 1984) are also plotted for comparison. The chondrite values are from Sun & McDonough (1989).

The results are presented using zircon morphology diagrams onto which their typology was plotted (Fig. 14). Although, great diversity of zircon types is obvious, the S-type zircons with dominant {101} pyramid and {100} prism prevail (Fig. 14). Most zircons have the length/width ratio ranging from 1.5–3 (Fig. 14).

Discussion

Sources of metasedimentary rocks

Monazite, xenotime and the spectrum of heavy earth minerals suggest that one major source for the Radlovac Complex metasedimentary rocks were felsic, igneous rocks of Variscan age. The Variscan age is supported by monazite from sample R1 (Table 2). From the high xenotime contents and Y-rich monazite, which suggest formation temperatures of >600–800 °C, it can be concluded that these Y-rich monazite grains come from a magmatic source because metamorphic rocks from the older surrounding complexes never experienced such high temperatures. In the case of monazite with lower Y-contents it is not clear if they come from magmatic or metamorphic rocks. However, it is important to note that the wide Y-, Th- and U spread observed in the monazite under study, is not untypical for grains, which formed in a magmatic milieu (e.g. Förster 1998; Förster et al. 2008).

Another argument therefore that the sediments were fed strongly by magmatic igneous rocks is the chemistry and morphology of type 1 xenotime. Type 1 xenotime can be interpreted as igneous-detrital, while type 2 xenotime is hydrothermal (Fig. 9). This is further confirmed by their discrepancy in chemistry. The observed zonation in type 1 xenotime (Fig. 8), which is, according to Kositcin et al.

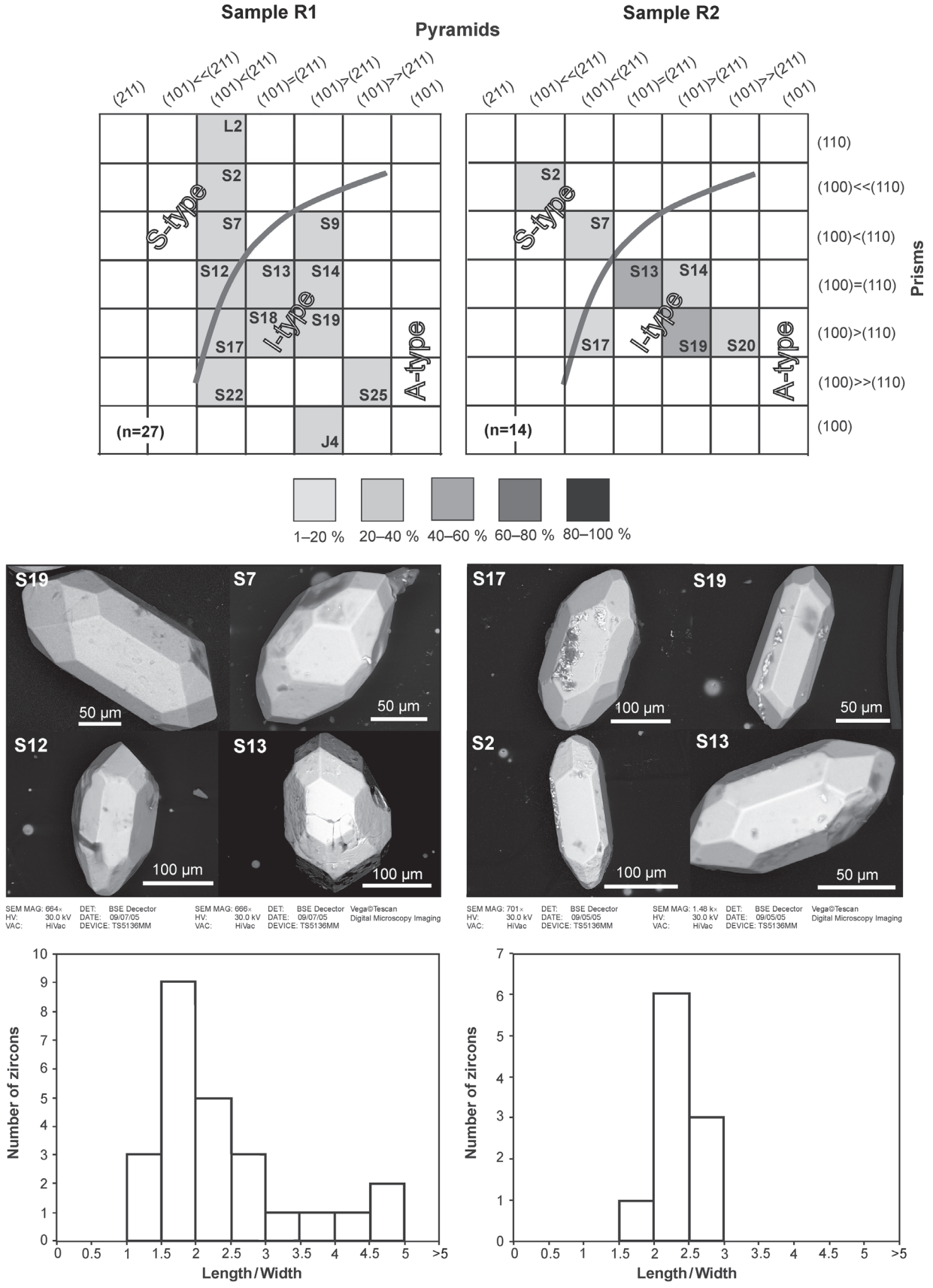

Fig. 14. Zircon typology diagrams for samples R1 and R2 together with some of the most abundant zircon types (after Pupin 1980) and Length/Width histograms. "n" refers to number of zircons analysed.

(2003), a direct consequence of variable degrees of substitution of HREEs, U and Th for Y during magmatic growth, is consistent with their igneous origin. This is in good correlation with xenotime data of varied origin (igneous, hydrothermal and diagenetic) known from the literature (Kositcin et al. 2003 and references therein) (Fig. 9). Diagenetic xenotime was not detected. Although, the xenotime grains were not suitable for dating due to low Th (especially hydrothermal grains), the igneous-detrital xenotime seems to be Variscan (Table 2) implying a Variscan igneous source consistent with the detrital monazite ages.

In the case of the hydrothermal xenotime it is possible that they formed during the Alpine metamorphism.

Monazite grains found in samples R15 are smaller and have lower Th and Y content indicative for low formation temperatures (e.g. Read et al. 1987; Rasmussen et al. 2001, 2007; Evans et al. 2002; Rasmussen & Muhling 2007, 2009; Wan et al. 2007; Wilby et al. 2007), all the more, as the bulk has relatively high Th and Y contents (Appendix). Bearing in mind the age dating and temperatures recorded on illite fractions presented in Biševac et al. (2009, 2010), we can assume that the population of Th- and Y-monazites found in sample R15 are Alpine (Cretaceous).

Heavy mineral assemblage

Heavy mineral analysis is one of the most sensitive and widely-used techniques for determination of the provenance of (meta)sedimentary rocks providing constraints on the mineralogical nature of the source terrains (Morton & Hallsworth 1999). The detrital heavy mineral assemblages of Radlovac Complex representative metapsammites are dominated by apatite and minerals like zircon, tourmaline and rutile. Additionally, minor quantity of epidote/zoisite, monazite and titanite can be found. Since the weathering of the parent rocks is a very important factor controlling the diversity of detrital heavy minerals in weathering profiles and later during sedimentation, the heavy mineral assemblage of Radlovac representative metapsammites indicate weathering-limited erosion. Under such conditions detritus is quickly removed without significant modification by chemical weathering (Johnsson et al. 1991), consistent with the presence of detrital apatite as the most abundant, but least stable mineral in weathering profile (Morton & Hallsworth 1999). Since apatite is a useful key mineral to detect the influence of acidic groundwater percolation and tends to be unstable under acidic conditions (Morton & Hallsworth 1999), its high abundance indicates the lack of acidic condition. The occurrence of other minerals (zircon, tourmaline and rutile) is not surprising since they show high stability in weathering profiles, but the presence of epidote/zoisite and lack of garnet and staurolite belonging to intermediate stability group (Morton & Hallsworth 1999) as well as, for example, pyroxenes, calcic amphibole or olivine indicate that metamorphic and/or basic igneous rocks did not serve as source rocks for the Radlovac Complex metasedimentary rocks. The presence of detrital igneous monazite and xenotime further argue for felsic igneous rocks as protolith.

Zircons occur both as irregular fragmented grains and as euhedral grains. The higher degree of roundness for some zircon grains than for quartz and feldspar grains in coarser-grained samples is probably the result of a minor degree of sedimentary recycling, since zircons are less prone to crystal growth during low-grade metamorphism than are quartz and feldspar (Augustsson & Bahlburg 2008). The euhedral to slightly abraded zircon originated mainly from I-type and subordinately S-type granites (Fig. 14), also indicating that the protolith material is characterized by shorter transportation paths. The length/width ratio of zircons show that they originated from magma characterized by slow to intermediate crystallization. The presence of euhedral zircons in association with prismatic crystals of tourmaline highlights the significance of the first-cycle input as well as short transportation.

Geochemistry

The variation of major elements between the two groups of samples (metapelites and metapsammites) primarily reflects the effect of grain size. Since metapelites contain more clay fraction it is expected to be richer in, for example, Al_2O_3, Fe_2O_3 or Na_2O. The bulk chemistry as well as La/Sc, Th/Sc, La/Co, Th/Co and Th/Cr values for both metapelites and metapsammites (Appendix), which are, according to Cullers (2000), indicative when evaluating source rocks, point to felsic igneous rocks as protolith for RC metasedimentary rocks. This is in good correlation with the heavy mineral assemblage discussed earlier and other discrimination diagrams (Figs. 10, 11 and 12). The diagram in Figure 12 shows that some metapsammite samples (R2 and R5) (Fig. 2) plot in the passive margin field (Fig. 12), which can indicate that they comprise felsic, old crustal, recycled detritus (Augustsson & Bahlburg 2008). The other metapsammite samples show a trend, which can be interpreted as due to temporal compositional variations of the provenance (Fig. 11).

Metapelites have a REE concentration and a Th/Sc, Th/Co and La/Sc similar to that of UCC (Fig. 11), while the REE concentrations for metapsammites are lower than UCC (Fig. 13) and Th/Sc, Th/Co and La/Sc values are higher than UCC (Appendix). Although, this could imply that metapsammites were partly affected by sedimentary recycling as discussed earlier, at least during the initial stages of Radlovac Complex sedimentation, we believe this is the direct consequence of Sc content controlled by grain-size, namely the abundant clay minerals in metapelites. Since Sc is often deposited in clay minerals together with iron and aluminium due to their similar ionic radius (Das et al. 1971), this is in good agreement with higher content of both Al_2O_3 and Fe_2O_3 (Appendix) in metapelites indicating the higher phyllosilicate content mostly related to the fine-grained matrix consisting predominately of illite-muscovite, chlorite and hematite. Eu anomalies ($Eu/Eu^* = 0.6–0.8$ for metapsammites; $Eu/Eu^* = 0.6–0.7$ for metapelites) are similar for both groups and reflect lithospheric or intracrustal fractionation or the breakdown of feldspar during weathering and/or metamorphic processes (see Condie et al. 1995).

Paleogeological settings

Paleogeological settings can be estimated on the basis of discrimination diagrams using major element and trace ele-

ment data. However, since the chemistry of the major elements can be modified in conditions of very low- to low-grade metamorphism due to their mobility, trace elements and lanthanides are frequently used for investigating the paleogeological setting of low-grade metasedimentary rocks. Elements such as La, Ce, Nd, Y, Th, Zr, Hf, Nb, Ti, and Sc are considered as the best indicators (Holland 1978; Bathia 1985; Bathia & Crook 1986; McLennan et al. 1993; Slack & Hoy 2000) and were used here to identify the geotectonic setting of the Radlovac metasedimentary rocks. Most of the samples plot into field of continental island arc, very similar to UCC and NASC (Fig. 12). In this geotectonic environment depositional basins were formed on a well-developed continental crust or thin continental margin. Sediments deposited along the continental island arc would be expected to be immature and less recycled due to smaller individual catchment areas, shorter transportation path and intermediate-quick storage which is in agreement with the chemical "signature" of the samples presented here. Comparison to data from the presently exposed surrounding basement rocks of the Slavonia Mts imply that local Variscan crust could serve as the protolith for the Radlovac Complex metasedimentary rocks (Fig. 12). Granitoid bodies of I- and S-type characteristic for the area together with migmatites and migmatitic gneisses characteristic for Papuk Complex served as the protolith for all the samples deposited in the continental island arc. Zircon typology studies of metapsammites of the Radlovac Complex (Fig. 14) compared with zircons of representative samples of Papuk Complex show great similarity and further confirm their genetic connection (Biševac 2009). Metapsammites characteristic for the lower part of the Radlovac Complex (R2 and R5) and granitoid rocks characteristic for Psunj Complex projected in passive margin field implying their genetic connection. This is in good agreement with the model proposed by Jamičić (1988) according to which the Psunj Complex rocks served as the dominant protolith during the initial phases of the Radlovac Complex sedimentation.

Conclusions

1. Monazite, xenotime and the spectrum of heavy earth minerals suggest that one major source for the Radlovac Complex metasedimentary rocks was felsic, igneous rocks of Variscan age. The Variscan age is supported by chemical Th-U-Pb monazite age dating. From the high xenotime contents and Y-rich monazite, which suggest formation temperatures of >600–800 °C, we can conclude that the Y-rich monazite grains come from a magmatic source.

2. The chemistry and morphology of type 1 xenotime (igneous-detrital) is another argument that the metasedimentary rocks of the Radlovac Complex were fed strongly by magmatic igneous rocks. Observed zonation in type 1 xenotime as a direct consequence of variable degrees of substitution of HREEs, U and Th for Y during magmatic growth, is consistent with their igneous origin. The igneous-detrital xenotime seems to be Variscan implying a Variscan igneous source consistent with the detrital monazite ages.

3. The detrital heavy mineral assemblages of the Radlovac Complex representative metapsammites are dominated by apatite and minerals like zircon, tourmaline and rutile accompanied by minor quantities of epidote/zoisite, monazite and titanite. Such assemblages further argue for felsic igneous rocks as protoliths.

4. The bulk chemistry as well as La/Sc, Th/Sc, La/Co, Th/Co and Th/Cr values for both metapelites and metapsammites point to felsic igneous rocks as protoliths for the Radlovac Complex metasedimentary rocks. This is in good correlation with the heavy mineral assemblage.

5. Elements such as La, Ce, Nd, Y, Th, Zr, Hf, Nb, Ti, and Sc were used to identify the geotectonic setting of the Radlovac metasedimentary rocks. Most of the samples plot into the field of continental island arcs, very similar to UCC and NASC. In this geotectonic environment depositional basins were formed on a well-developed continental crust or thin continental margin.

6. Comparison to the presently exposed surrounding basement rocks of the Slavonian Mts, data implies that local Variscan crust could serve as protolith for the Radlovac Complex metasedimentary rocks. The granitoid bodies of I- and S-type characteristic for the area together with migmatites and migmatitic gneisses characteristic for Papuk Complex served as protolith for all samples deposited in the continental island arc.

7. The provenance study of the RC metasedimentary rocks based on Th-U-Pb monazite chemical age dating, heavy mineral assemblage and whole-rock geochemistry leads to the conclusion that the metasedimentary rocks of the Radlovac Complex represent the detritus of the local Variscan crust, while Papuk Complex rocks were dominant source material.

8. The identification of the provenance in this study resulted from combination of several independent analytical techniques supporting the importance of combining different methods in provenance studies.

Acknowledgments: The authors would like to thank the reviewers for their stimulating and constructive comments, as well as the Editor for handling the manuscript. This study was supported by the Croatian Ministry of Science, Education and Sports, Project No. 119-1191155-1156 and by the Austrian Science Foundation (FWF), Project No. 22408.

References

Augustsson C. & Bahlburg H. 2008: Provenance of late Palaeozoic metasediments of the Patagonian proto-Pacific margin (southernmost Chile and Argentina). *Int. J. Earth Sci. (Geol. Rundsch.)* 97, 71–88.

Balen D., Horváth P., Tomljenović B., Finger F., Humer B., Pamić J. & Árkai P. 2006: A record of pre-Variscian Barrovian regional metamorphism in the eastern part of Slavonian Mountains (NE Croatia). *Miner. Petrology* 87, 143–162.

Bathia M.R. 1985: Rare element geochemistry of Australian Paleozoic greywackes and mudrocks: Provenance and tectonic control. *Sed. Geol. 45*, 97–113.

Bathia M.R. & Crook K.A.W. 1986: Trace elements characteristics of graywackes and tectonic setting discriminations of sedimentary basins. *Contr. Mineral. Petrology* 92, 181–193.

Biševac V. 2009: Provenance, age and degree of metamorphism of

the Radlovac metamorphic complex. *PhD Thesis, Univ. Zagreb*, 1–304 (in Croatian).

Biševac V., Balen D., Tibljaš D. & Španić D. 2009: Preliminary results on degree of thermal alteration recorded in the eastern part of Mt. Papuk, Slavonia, Croatia. *Geol. Croatica* 62, 1, 63–71.

Biševac V., Balogh K., Balen D. & Tibljaš D. 2010: Eoalpine (Cretaceous) very low- to low-grade metamorphism recorded on the illite-muscovite-rich fraction of metasediments from South Tisia (eastern Mt Papuk, Croatia). *Geol. Carpathica* 61, 6, 469–481.

Biševac V., Krenn E., Balen D., Finger F. & Balogh K. 2011: Petrographic, geochemical and geochronological investigation on granitic pebbles from Permotriassic metasediments of the Tisia terrain (eastern Papuk). *Miner. Petrology* 102, 163–180.

Brkić M., Jamičić D. & Pantić N. 1974: Carboniferous deposits in Mount Papuk (northeastern Croatia). *Geol. Vjes.* 27, 53–58 (in Croatian).

Bucher L. & Frey M. 1994: Petrogenesis of metamorphic rocks. 6th edition. *Springer Verlag*, Berlin, 1–318.

Condie K.C., Dengate J. & Cullers R.L. 1995: Behavior of rare earth elements in a paleoweathering profile on granodiorite in the front range, Colorado, USA. *Geochim. Cosmochim. Acta* 59, 279–294.

Csontos L. 1995: Tertiary tectonic evolution of the Intra-Carpathian area: a review. *Acta Vulcanol.* 7, 1–13.

Csontos L. & Vörös A. 2004: Mesozoic plate tectonics reconstruction of the Carpathian region. *Palaeogeogr. Palaeoclimatol. Palaeoecol.* 210, 1–56.

Cullers R.L. 2000: The geochemistry of shales, siltstones and sandstones of Pennsylvanian-Permian age, Colorado, U.S.A.: implications for provenance and metamorphic studies. *Lithos* 51, 305–327.

Cullers R.L. 2002: Implications of elemental concentrations for provenance, redox conditions, and metamorphic studies of shales and limestones near Pueblo, CO, USA. *Chem. Geol.* 191, 4, 305–327.

Das H.A., Zonderhuis I. & Marel H.W. van der 1971: Scandium in rocks, minerlas and sediments and its relations to iron and aluminium. *Contr. Mineral. Petrology* 32, 231–244.

Evans J.A., Jalasiewicz J.A., Fletcher I.R., Rasmussen B. & Pearce N.J.G. 2002: Dating diagenetic monazite in mudrocks: constraining the oil window? *Geol. Soc., Spec. Publ.* 159, 619–622.

Förster H.J. 1998: The chemical composition of REE-Y-Th-U rich accessory minerals from the peraluminous granits from the Erzgebirge-Fichtelgebirge region, German. Part 1: The monazite- (Ce)-brabantite solid solution series. *Amer. Mineralogist* 83, 259–273.

Förster H.J., Rhede D. & Hecht L. 2008: Chemical composition of radioactive accessory minerals: implications for the evolution, alteration, age, and uranium fertility of the Fichtelgebirge granites (NE Bavaria, Germany). *Neu. Jb. Mineral. Abh.* 185, 161–182.

Frimmel H.E. 1994: Metamorphism of Witwatersrand gold. *Exploration and Mining Geology* 3, 357–370.

Fülöp J., Brezsnyansky K. & Hass J. 1987: The new map of basin basement of Hungary. *Acta Geol. Hung.* 30, 3–20.

Géczy B. 1973: The origin of the Jurassic faunal provinces and the Mediterranean plate tectonics. *Ann. Univ. Sci. Budapest, Eötvös Nom. Sect. Geol.* 16, 99–114.

Gratz R. & Heinrich W. 1997: Monazite-xenotime thermobarometry: experimental calibration of the miscibility gap in the system $CePO_4$–YPO_4. *Amer. Mineralogist* 82, 772–780.

Gromet L.P., Dymek R.F., Haskin L.A. & Korotev R.F. 1984: The "North American shale composite": its compilation, major and trace element characteristics. *Geochim. Cosmochim. Acta* 48, 2469–2482.

Haas J. & Péró C. 2004: Mesozoic evolution of the Tisza Megaunit. *Int. J. Earth Sci. (Geol. Rundsch.)* 93, 297–313.

Haas J., Mioč P., Pamić J., Tomljenović B., Árkai P., Berzcki-Makk A., Koronkai B., Kovács S. & Felgenkauer E.R. 2000: Complex strucutre pattern of the Alpine-Dinnaridic-Pannonian triple junction. *Int. J. Earth Sci. (Geol. Rundsch.)* 89, 377–389.

Hallsworth C.R., Morton A.C., Claoue'-Long J. & Fanning C.M. 2000: Carboniferous sand provenance in the Pennine Basin, UK: constraints from heavy mineral and detrital zircon age data. *Sed. Geol.* 137, 147–185.

Heinrich W., Andrehs G. & Franz G. 1997: Monazite–xenotime miscibility gap thermometry. I. An empirical calibration. *J. Metamorph. Geology* 15, 3–16.

Holland H.D. 1978: The chemistry of the atmosphere and oceans. *Wiley*, New York, 1–351.

Horváth P., Balen D., Finger F., Tomljenović B. & Krenn E. 2010: Contrasting P-T-t paths from the basement of the Tisia Unit (Slavonian Mts., NE Croatia): application of quantitative phase diagrams and monazite age dating. *Lithos* 117, 269–282.

Jamičić D. 1983: Structural fabric of the metamorphosed rocks of Mt. Krndija and the eastern part of Mt. Papuk. *Geol. Vjes.* 36, 51–72 (in Croatian).

Jamičić D. 1988: Structural fabric of the Slavonian Mts. (northern Papuk, Psunj, Krndija). *PhD Thesis, Univ. Zagreb*, 1–152 (in Croatian).

Jamičić D. & Brkić M. 1987: Basic Geological Map of Yugoslavia in scale 1:100,000, sheet Orahovica L 33–96. *Sav. Geol. Inst.*, Beograd.

Jamičić D., Brkić M., Crnko J. & Vragović M. 1987: Basic Geological Map of Yugoslavia — Explanatory notes for sheet Orahovica L 33–96. *Fed. Geol. Inst. Beograd*, 1–72 (in Croatian).

Johnsson M.J., Stallard R.F. & Lundberg N. 1991: Controls on the composition of fluvial sands from a tropical weathering environment: Sands of the Orinoco drainage basin, Venezuela and Colombia. *Bull. Geol. Soc. Amer.* 103, 1622–1647.

Kositcin N., McNaughton N.J., Griffin B.J., Fletcher I.R., Groves D.I. & Rasmussen B. 2003: Textural and geochemical discrimination between xenotime of different origin in the Archaean Witwatersrand Basin, South Africa. *Geochim. Cosmochim. Acta* 67, 709–731.

Krenn E., Ustaszewski K. & Finger F. 2008: Detrital and newly formed metamorphic monazite in amphibolite-facies metapelites from the Motajica Massif, Bosnia. *Chem. Geol.* 254, 164–174.

Ludwig K.R. 2001: Isoplot/Ex, Version 2.49e. A Geochronological Toolkit for Microsoft Excel. *Berkeley Geochronological Center Special Publications.*

Mange M.A. & Maurer H.F.W. 1991: Heavy minerals in colour. *Chapman and Hall*, London, 1–147.

Márton E. 2000: The Tisza Megatectonic Unit in the light of paleomagnetic data. *Acta Geol. Hung.* 43, 3, 329–343.

Márton E. 2001: Tectonic implications of Tertiary paleomagnetic results from the PANCARDI area (Hungarian contribution). *Acta Geol. Hung.* 44, 135–144.

McLennan S.M., Hemming S., McDaniel D.K. & Hanson G.N. 1993: Gechemical approaches to sedimentation, provenance and tectonics. In: Johnsson M.J. & Basu A. (Eds.): Processes controlling the composition of clastic sediments. *Geol. Soc. Amer., Spec. Pap.* 284, 21–40.

Meinhold G., Kostopoulos D. & Reischmann T. 2007: Geochemical constraints on the provenance and depositional setting of sedimentary rocks from the islands of Chios, Inousses and Psara, Aegean Sea, Greece: implications for the evolution of Palaeotethys. *J. Geol. Soc. London* 164, 1145–1163.

Mikes T., Christ D., Petri R., Dunkl I., Frei D., Báldi-Beke M., Reitner J., Wemmer K., Hrvatović H. & von Eynatten H. 2008: Provenance of the Bosnian Flysch. *Swiss J. Geosci.* 101, 1, 31–54.

Montel J.M., Foret S., Veschambre M., Nicollet C. & Provost A.

1996: Electron microprobe dating of monazite. *Chem. Geol.* 131, 37–53.

Morton A.C. & Hallsworth C.R. 1999: Processes controlling the composition of heavy mineral assemblages in sandstones. *Sed. Geol.* 124, 3–29.

Pamić J. 1986: Magmatic and metamorphic complexes of the adjoining area of the northernmost Dinarides and Pannonian Mass. *Acta Geol. Hung.* 29, 203–220.

Pamić J. 1998: Crystalline basement of the South Pannonian Basin based on surface and subsurface data. *Nafta* 49, 371–390.

Pamić J. & Jamičić D. 1986: Metabasic intrusive rocks from the Paleozoic Radlovac complex of Mt. Papuk in Slavonija (northern Croatia). *Rad JAZU* 424, 97–125.

Pamić J. & Lanphere M. 1991: Hercynian granites and metamorphic rocks of the Mts. Papuk, Psunj, Krndija and surrounding basement of the Pannonian Basin, North Croatia. *Monograph. Geologija* 34, 81–235 (in Croatian).

Pamić J. & Jurković I. 2002: Paleozoic tectonostratigraphic units of the northwest and central Dinarides and the adjoining South Tisia. *Int. J. Earth Sci.* 91, 538–554.

Pamić J., Lanphere M. & McKee E. 1988: Radiometric ages of metamorphic and associated igneous rocks of the Slavonian Mountains in the southern part of Pannonian Basin, Yugoslavia. *Acta Geol.* 18, 13–39.

Pamić J., Lanphere M. & Belak M. 1996: Hercynian I-type and S-type granitoids from the Slavonian Mountains (southern Pannonian, north Croatia). *Neu. Jb. Mineral. Abh.* 171, 155–186.

Pamić J., Balen D. & Tibljaš D. 2002: Petrology and geochemistry of orthoamphibolites from the Variscan metamorphic sequences of the South Tisia in Croatia — an overview with geodynamic implications. *Int. J. Earth Sci.* 91, 787–798.

Pupin J.P. 1980: Zircon and granite petrology. *Contr. Mineral. Petrology* 73, 207–220.

Pyle J.M., Spear F.S., Rudnick R.L. & McDonough W.F. 2001: Monazite–xenotime garnet equilibrium in metapelites and a new monazite-garnet thermometer. *J. Petrology* 42, 2083–2107.

Rasmussen B. & Muhling J.R. 2007: Monazite begets monazite: evidence for dissolution of detrital monazite and reprecipitation of syntectonic monazite during low-grade regional metamorphism. *Contr. Mineral. Petrology* 154, 675–689.

Rasmussen B. & Muhling J.R. 2009: Reactions destroying detrital monazite in greenschist-facies sandstones from the Witwatersrand basin, South Africa. *Chem. Geol.* 264, 311–327.

Rasmussen B., Fletcher I.R. & McNaughton N.J. 2001: Dating low grade metamorphic events by SHRIMP U–Pb analysis of monazite in shales. *Geology* 29, 963–966.

Rasmussen B., Fletcher I.R. & Muhling J.R. 2007: In situ U-Pb dating and element mapping of three generations of monazite: unravelling cryptic tectonothermal events in low-grade terranes. *Geochim. Cosmochim. Acta* 71, 670–690.

Read D., Cooper D.C. & McArthur J.M. 1987: The composition and distribution of nodular monazite in the Lower Palaeozoic rocks of Great Britain. *Mineral. Mag.* 51, 271–280.

Roser B.P. & Korsch R.J. 1988: Provenance signatures of sandstone-mudstone suites determined using discriminant function analysis of major-element data. *Chem. Geol.* 67, 119–139.

Schmid S.M., Bernoulli D., Fügenschuh B., Matenco L., Schefer S., Schuster R., Tischler M. & Ustaszewski K. 2008: The Alpine-Carpathian-Dinaridic orogenic system: correlation and evolution of tectonic units. *Swiss J. Sci.* 101, 139–183.

Slack J.F. & Höy T. 2000: Geochemistry and provenance of clastic metasedimentary rocks of the Aldridge and Fort Steele Formation, Purcell Supergroup, SE British Columbia. In: Lydon J.W., Höy T., Slack J.F. & Knapp M.E. (Eds.): The geological enviroment of the Sullivan Deposit, British Columbia. *GAC, Spec. Publ.* 1, 180–201.

Stampfli G.M., Borel G.D., Marchant R. & Mosar J. 2002: Western Alps geological constraints on western Tethyan reconstructions. *J. Virtual Explorer* 8, 77–106.

Sun S. & McDonough W.F. 1989: Chemical and isotopic systematics of oceanic basalts: implications for mantle composition and processes. In: Saunders A.D. & Norry M.J. (Eds.): Magmatism in the Ocean Basins. *Geol. Soc. London, Spec. Publ.* 42, 313–345.

Sutton S.J., Ritger S.D. & Maynard J.B. 1990: Stratigraphic control of chemistry and mineralogy in metamorphosed Witwatersrand quartzites. *J. Geol.* 98, 329–341.

Suzuki K., Adachi M. & Tanaka T. 1991: Middle Precambrian provenance of Jurassic sandstone in the Mino Terrane, central Japan: Th-U-total Pb evidence from an electron microprobe monazite study. *Sed. Geol.* 75, 141–147.

Tari V. & Pamić J. 1998: Geodynamic evolution of the northern Dinarides and south Pannonian basin. *Tectonophysics* 297, 269–281.

Taylor S.R. & McLennan S.M. 1985: The continental crust: Its composition and evolution. *Blackwell,* Oxford, 1–312.

von Eynatten H. 2003: Petrography and chemistry of sandstones from the Swiss Molasse Basin: an archive of the Oligocene to Miocene evolution of the Central Alps. *Sedimentology* 50, 703–724.

von Eynatten H. & Wijbrans J.R. 2003: Precise tracing of exhumation and provenance using $^{40}Ar/^{39}Ar$ geochronology of detrital white mica: the example of the Central Alps. In: McCann T. & Saintot A. (Eds.): Tracing tectonic deformation using the sedimentary record. *Geol. Soc. London, Spec. Publ.* 208, 289–305.

Wan Y.S., Song T.R., Liu D.Y., Yang T.N., Yin X.Y., Chen Z.Y. & Zhang Q.D. 2007: Mesozoic monazite in Neoproterozoic metasediments: Evidence for low-grade metamorphism of Sinian sediments during Triassic continental collision, Liaodong Peninsula, NE China. *Geochem. J.* 41, 47–55.

Weltje G.J. & von Eynatten H. 2004: Quantitative provenance analysis of sediments: review and outlook. *Sed. Geol.* 171, 1–11.

Whitney D.L & Evans B.W. 2010: Abbreviations for names of rock-forming minerals. *Amer. Mineralogist* 95, 185–187.

Wilby P.R., Page A.A., Zalasiewicz J.A., Milodowski A., Eliams M. & Evans J.A. 2007: Syntectonic monazite in low-grade mudrocks: a potential geochronometer for cleavage formation? *J. Geol. Soc.* 164, 53–56.

Willan R.C.R. 2003: Provenance of Triassic-Cretaceous sandstones in the Antarctic Peninsula: implications for terrane models during Gondwana breakup. *J. Sed. Res.* 73, 1062–1077.

Willner A.P., Ermolaeva T., Stroink L., Glasmacher U.A., Giese U., Puchkov V.N., Kozlov V.I. & Walter R. 2001: Contrasting provenance signals in Riphean and Vendian sandstones in the SW Urals (Russia): constraints for a change from passive to active continental margin conditions in the Neoproterozoic. *Precamb. Res.* 110, 215–239.

York D. 1966: Least squares fitting of a straight line. *Canad. J. Phy.* 44, 1079–1086.

Zack T., von Eynatten H. & Kronz A. 2004: Rutile geochemistry and its potential use in quantitative provenance studies. *Sed. Geol.* 171, 37–58.

Appendix

Chemical data for metasedimentary rocks belonging to the Radlovac complex, as well as for representative samples from Psunj and Papuk complexes used here for comparison as possible protolith.

Radlovac Complex metasedimentary rocks																	
		Metapelite								Metapsammites							
Sample		**R1**	**R2**	**R3**	**R4**	**R5**	**R6**	**R7**	**R8**	**R9**	**R10**	**R11**	**R12**	**R13**	**R14**	**R15**	**R16**
Element	d.l. (wt. %)																
SiO_2	0.01	77.38	75.52	64.99	76.83	77.2	60.88	63.57	67.91	62.53	56.73	58.38	58.73	56.98	56.94	53.55	49.14
Al_2O_3	0.01	13.86	9.93	15.51	14.3	11.61	17.56	18.6	17.24	19.7	14.41	18.5	18.36	19.67	19.31	24.79	27.79
Fe_2O_3	0.04	1.21	0.96	5.31	1.05	0.76	6.42	4.57	3.1	6.25	5.48	7.29	7.09	7.19	7.55	6.93	6.73
MgO	0.01	0.37	0.41	3.76	0.35	0.33	3.18	2.07	2.01	0.75	2.59	3.49	3.16	3.19	3.5	1.79	1.36
CaO	0.01	0.12	4.18	0.64	0.1	2.01	0.45	0.33	0.11	0.11	6.83	0.89	0.88	0.34	0.33	0.15	0.22
Na_2O	0.01	1.25	0.9	2.53	1.17	0.72	2.09	1.4	2.68	2.16	1.81	2.99	3.94	3.19	2.54	1.28	1.78
K_2O	0.01	2.9	2.47	2.58	3.06	3.17	4.38	4.09	2.95	4.13	2.32	3.65	3.05	4.07	4.34	5.36	3.61
TiO_2	0.01	0.56	0.18	0.76	0.55	0.22	1.18	0.62	0.53	0.87	0.55	0.71	0.72	0.87	0.74	0.98	0.99
P_2O_5	0.01	0.07	0.07	0.08	0.08	0.08	0.31	0.08	0.07	0.07	0.14	0.23	0.19	0.25	0.2	0.09	0.14
MnO	0.01	<0.01	0.04	0.02	<0.01	0.02	0.03	0.03	0.02	0.02	0.18	0.12	0.04	0.07	0.11	0.05	0.03
LOI	0.01	2.2	5.3	3.6	2.4	3.8	3.3	4.4	3.2	3.2	8.8	3.6	3.7	4	4.2	4.8	8
Total		99.92	99.96	99.78	99.89	99.92	99.78	99.76	99.82	99.79	99.84	99.85	99.86	99.82	99.76	99.77	99.79
	d.l. (ppm)																
As	0.5	5.8	30	1.3	3.5	1.6	0.5	1.2	<d.l.	1	18.8	6	4.9	5.5	19.7	1.3	15.9
Au	0.5**	1.8	<d.l.	0.9	<d.l.	1.6	3.6	1.4	2.6	6	<d.l.	0.8	1	12.1	<d.l.	1.3	1.8
Ba	1	575	359	601	583	458	646	1076	794	886	661	481	297	453	564	1096	764
Be	1	2	3	3	3	2	<d.l.	3	3	3	2	3	2	4	3	4	5
Co	0.2	4.2	1.2	10.9	4.2	0.6	21.6	8.8	7.1	8.7	9.3	19.6	16.7	18.5	17.6	16.8	7.7
Cr	20	50	20	80	50	30	150	80	50	80	80	120	130	140	150	120	110
Cs	0.1	13.1	11.4	4.9	21.4	16.6	15.6	13.1	7.7	4	4.4	7	4.2	9.5	3.9	4.9	5.6
Cu	0.1	3.8	7.1	1.1	2.1	4.8	1.9	0.4	0.9	1.4	17.4	17.2	0.5	15.7	23	0.3	21.3
Ga	0.5	14.1	10.8	16.3	15.2	11.2	19.8	22.9	21.5	23.3	17.2	24.6	23	24.3	25.2	30.6	31.9
Hg	0.01	<d.l.	0.27	0.01	<d.l.	0.06	<d.l.	<d.l.	0.01	<d.l.	0.04	<d.l.	<d.l.	<d.l.	<d.l.	<d.l.	0.16
Hf	0.1	4.1	2.8	8.4	4.6	3.5	6.1	6.5	3.5	7.1	5.7	4.8	4.8	5.3	5	6.1	7.6
Mo	0.1	<d.l.	<d.l.	<d.l.	<d.l.	<d.l.	<d.l.	<d.l.	<d.l.	<d.l.	<d.l.	0.1	<d.l.	0.1	0.1	<d.l.	0.5
Nb	0.1	8.8	3	11.8	8.6	3.8	11.3	10.2	9.6	12.4	11.8	15.3	14.8	16.3	15.5	15.4	14.9
Ni	0.1	6.9	3.2	26.7	6.4	2.4	49.7	12.2	9.2	28.3	22.7	40.1	37.1	43.6	42.3	39.7	31.5
Pb	0.1	3.8	7.1	1.1	2.1	4.8	1.9	0.4	0.9	1.4	17.4	17.2	0.5	15.7	23	0.3	21.3
Rb	0.1	105.4	63.7	88.7	111.6	81.6	129.4	163.4	106.8	148.9	90.2	154.7	133.7	175.1	194.4	206.7	144.5
Sb	0.1	0.2	<d.l.	<d.l.	0.1	<d.l.	0.3	0.2	<d.l.	0.8	0.4	0.5	0.3	0.5	0.3	0.5	0.2
Sc	1	7	3	12	7	3	21	10	8	16	11	17	17	20	20	19	18
Sn	1	2	<d.l.	2	1	1	3	3	2	3	3	6	5	5	5	5	5
Sr	0.5	71.5	81.9	66.2	70.7	49.4	43.6	49.5	71.9	131.5	196.7	64.1	54.1	46.3	48.7	141.8	193.8
Ta	0.1	0.8	0.3	0.7	0.9	0.5	0.8	0.8	0.8	1.1	1	1.4	1.1	1.4	1.3	1.1	1.3
Th	0.2	9.2	6.6	8.5	10.4	7.5	8.7	11.3	9.4	13.6	11.1	16.5	14.8	16.6	16.3	14.8	16.6
Tl	0.1	<d.l.	<d.l.	<d.l.	<d.l.	<d.l.	0.1	0.2	<d.l.	0.1	0.1	0.1	<d.l.	0.1	0.1	0.2	<d.l.
U	0.1	2.5	1.1	2.3	2.6	1.3	2.5	1.9	1.7	2.2	3.3	7.4	5	5.9	6.1	3.1	5.4
V	2	49	19	91	55	20	85	53	67	73	69	134	103	164	112	120	119
W	0.5	<d.l.	0.5	0.7	1.3	1	0.8	1	1.1	2.1	1.2	2.9	2.8	3.5	3.1	2.5	3

** — ppb; **<d.l.** — below detection limit

Appendix (continued)

Radlovac Complex metasedimentary rocks																	
		Metapelite								Metapsammites							
Sample		**R1**	**R2**	**R3**	**R4**	**R5**	**R6**	**R7**	**R8**	**R9**	**R10**	**R11**	**R12**	**R13**	**R14**	**R15**	**R16**
Element	d.l. (ppm)																
Y	0.1	10.9	13	22.2	14.2	10.4	31.2	13.8	8.8	20.5	23.1	36.4	30.8	37.1	35	31.4	28.9
Zn	1	7	24	96	6	11	52	60	55	49	59	132	118	116	106	86	58
Zr	0.1	143.9	86.3	273.9	152.1	118.3	243.2	233.8	130.3	231.3	179	148.1	156.7	171.1	162.1	203.9	241.7
La	0.1	28.4	18.3	28.1	28.3	22.9	22.8	37	27.1	37.4	30.1	45.4	39.3	46.8	46.1	47.5	44.3
Ce	0.1	53.7	36.9	56.5	55.4	46.6	47.8	73	53.5	77.2	60.7	93.2	83.8	95	94.2	102.1	90.9
Pr	0.02	6.13	4.32	6.92	6.52	5.34	6.23	8.17	6.14	8.89	6.85	11.21	9.3	11.03	11	11.31	11.14
Nd	0.3	22.1	15.8	25.8	23.9	19.7	24.1	29.1	22.2	32.8	25.9	42.7	33.4	42	40.9	43.6	41.1
Sm	0.05	3.63	3.1	5.32	4.18	3.4	5.53	4.87	3.75	6.32	5.21	8.71	6.74	8.44	8.28	8.2	7.73
Eu	0.02	0.66	0.66	1.17	0.7	0.68	1.24	1.08	0.84	1.43	0.86	1.65	1.19	1.58	1.43	1.84	1.58
Gd	0.05	2.61	2.78	4.59	3.04	2.31	5.55	3.4	2.32	4.92	4.34	7.77	6.15	7.5	7.36	6.97	6.04
Tb	0.01	0.39	0.45	0.74	0.43	0.34	0.88	0.47	0.33	0.76	0.75	1.29	1.01	1.22	1.21	1.14	1.00
Dy	0.05	2.14	2.58	4.33	2.7	1.95	5.26	2.38	1.73	4.17	4.06	6.88	5.54	6.83	6.64	6.13	5.44
Ho	0.02	0.39	0.49	0.84	0.45	0.37	1.1	0.47	0.3	0.81	0.9	1.38	1.16	1.34	1.34	1.19	1.17
Er	0.03	1.28	1.29	2.49	1.25	1.12	3.18	1.33	0.86	2.46	2.67	3.67	3.05	3.78	3.59	3.23	3.32
Tm	0.01	0.2	0.19	0.4	0.24	0.17	0.47	0.22	0.13	0.35	0.42	0.57	0.48	0.57	0.55	0.51	0.48
Yb	0.05	1.31	1.2	2.4	1.52	1.11	3.12	1.41	0.9	2.33	2.56	3.63	2.91	3.43	3.49	3.33	3.15
Lu	0.01	0.2	0.18	0.38	0.2	0.16	0.44	0.21	0.14	0.36	0.4	0.52	0.46	0.52	0.52	0.49	0.48
∑ REEs		123.1	88.24	140	128.8	106.2	127.7	163.1	120.2	180.2	145.7	228.6	194.5	230	226.6	237.5	217.8
Eu/Eu*		0.65	0.68	0.72	0.59	0.73	0.68	0.80	0.86	0.78	0.55	0.61	0.56	0.60	0.55	0.74	0.70
A/CNK		3.25	1.32	2.70	3.30	1.97	2.54	3.20	3.00	3.08	1.31	2.46	2.33	2.59	2.68	3.65	4.95
La/Co		6.76	15.25	2.58	6.74	38.17	1.06	4.20	3.82	4.30	3.24	2.32	2.35	2.53	2.62	2.83	5.75
Th/Co		2.19	5.50	0.78	2.48	12.50	0.40	1.28	1.32	1.56	1.19	0.84	0.89	0.90	0.93	0.88	2.16
Th/Sc		1.31	2.20	0.71	1.49	2.50	0.41	1.13	1.18	0.85	1.01	0.97	0.87	0.83	0.82	0.78	0.92
La/Sc		4.06	6.10	2.34	4.04	7.63	1.09	3.70	3.39	2.34	2.74	2.67	2.31	2.34	2.31	2.50	2.46
Th/Cr		0.18	0.33	0.11	0.21	0.25	0.06	0.14	0.19	0.17	0.14	0.14	0.11	0.12	0.11	0.12	0.15
Y/Ni		1.58	4.06	0.83	2.22	4.33	0.63	1.13	0.96	0.72	1.02	0.91	0.83	0.85	0.83	0.79	0.92
Cr/V		1.02	1.05	0.88	0.91	1.50	1.76	1.51	0.75	1.10	1.16	0.90	1.26	0.85	1.34	1.00	0.92
Zr/Sc		20.56	28.77	22.83	21.73	39.43	11.58	23.38	16.29	14.46	16.27	8.71	9.22	8.56	8.11	10.73	13.43
Hf/Sc		0.59	0.93	0.70	0.66	1.17	0.29	0.65	0.44	0.44	0.52	0.28	0.28	0.27	0.25	0.32	0.42

Appendix (continued)

		Papuk Complex				Psunj Complex		
Sample		**granite**	**granite**	**gneiss**	**gneiss**	**granite**	**granite**	**granite**
Element	d.l. (wt. %)							
SiO_2	0.01	74.33	67.59	74.46	70.44	56.12	72.08	74.08
Al_2O_3	0.01	13.91	16.23	12.39	13.68	20.17	14.03	12.68
Fe_2O_3	0.04	1.33	3.4	2.59	4.43	6.08	2.43	2.83
MgO	0.01	0.43	1.54	0.72	1.91	2.16	0.51	0.4
CaO	0.01	1.18	1.97	0.66	1.18	5.79	1.89	0.9
Na_2O	0.01	3.86	3.75	3.71	2.58	4.87	4.41	4.61
K_2O	0.01	3.92	2.88	3.39	2.79	1.12	2.93	3.05
TiO_2	0.01	0.14	0.49	0.34	0.7	1.02	0.31	0.3
P_2O_5	0.01	0.07	0.2	0.07	0.11	0.28	0.07	0.08
MnO	0.01	0.03	0.08	0.02	0.04	0.1	0.03	0.03
LOI	0.01	0.7	1.7	1.5	2	2.1	1.2	0.9
Total		99.92	99.86	99.88	99.86	99.8	99.86	99.87
	d.l. (ppm)							
As	0.5	0.6	0.9	<d.l.	<d.l.	<d.l.	<d.l.	<d.l.
Au	0.5**	6.1	1.1	2	1.8	<d.l.	1.9	0.5
Ba	1	584	526	227	426	331	831	573
Be	1	3	4	4	<d.l.	2	2	2
Co	0.2	1.6	6.1	1.6	10.8	8.2	2.4	2.1
Cr	20	40	50	30	90	30	<d.l.	<d.l.
Cs	0.1	4.2	6.5	1	5.1	0.7	0.4	2.7
Cu	0.1	0.6	5.1	0.6	1	10.4	1.3	0.7
Ga	0.5	14	19.8	15.8	14.4	20.5	20	21.3
Hg	0.01	<d.l.	0.02	<d.l.	0.03	<d.l.	0.01	0.01
Hf	0.1	2.1	5.2	6.4	6.1	6.5	6.4	11.6
Mo	0.1	<d.l.	<d.l.	0.1	<d.l.	<d.l.	<d.l.	0.2
Nb	0.1	6.9	11.2	9.7	9.8	4.2	8.9	17.3
Ni	0.1	3.5	10.1	2	25.5	2.7	1.6	1.8
Pb	0.1	7.6	2.7	1.9	2.2	9.6	5.1	3.2
Rb	0.1	111.5	126	117.1	113.4	35	55.7	70.6
Sb	0.1	<d.l.	0.1	<d.l.	<d.l.	<d.l.	<d.l.	<d.l.
Sc	1	6	7	8	13	11	5	4
Sn	1	2	5	19	1	1	1	2
Sr	0.5	144.9	311.4	47.8	169.8	664.3	133.6	85.7
Ta	0.1	1	1.2	0.7	0.7	0.3	0.4	0.9
Th	0.2	4.8	10.2	25.4	7.6	1.7	14.2	10.5

		Papuk Complex				Psunj Complex		
Sample		**granite**	**granite**	**gneiss**	**gneiss**	**granite**	**granite**	**granite**
Element	d.l. (ppm)							
Tl	0.1	0.2	0.4	<d.l.	0.5	<d.l.	0.1	0.3
U	0.1	4.5	2.2	1.9	2	0.7	2.3	3.2
V	2	13	57	45	103	91	20	19
W	0.5	<d.l.	<d.l.	1.7	<d.l.	<d.l.	<d.l.	<d.l.
Y	0.1	16.9	10.2	43.1	24.2	19.6	21.5	79.8
Zn	1	26	53	15	62	59	25	66
Zr	0.1	59	175.2	186.4	213.1	270.9	227.6	387.9
La	0.1	7.9	32.3	45.3	30.4	13.9	39.6	33.7
Ce	0.1	16.9	61.5	98.3	60.3	26.4	74.7	71.3
Pr	0.02	2.09	6.86	11.08	7.15	4.01	8.73	10.12
Nd	0.3	7.7	24.7	40.7	27.2	17	31.2	43.8
Sm	0.05	1.91	3.7	8.12	5.15	3.93	5.9	12.88
Eu	0.02	0.6	1.02	0.51	1.08	1.34	1.07	1.06
Gd	0.05	1.97	2.36	7.51	4.54	3.99	5.02	15.15
Tb	0.01	0.39	0.35	1.31	0.71	0.67	0.77	2.7
Dy	0.05	2.53	1.81	7.49	4.14	3.66	4.07	16.02
Ho	0.02	0.58	0.35	1.51	0.86	0.74	0.82	3.14
Er	0.03	1.83	1.01	4.18	2.46	2.08	2.16	8.72
Tm	0.01	0.31	0.17	0.6	0.38	0.31	0.3	1.22
Yb	0.05	2.26	1.07	3.34	2.43	2.11	1.8	7.62
Lu	0.01	0.37	0.18	0.52	0.38	0.32	0.28	1.13
∑ REEs		47.34	137.4	230.5	147.2	80.46	176.4	228.6
Eu/Eu*		0.94	1.04	0.20	0.68	1.02	0.59	0.23
A/CNK		1.55	1.89	1.60	2.09	1.71	1.52	1.48
La/Co		4.94	5.30	28.31	2.81	1.70	16.50	16.05
Th/Co		3.00	1.67	15.88	0.70	0.21	5.92	5.00
Th/Sc		0.80	1.46	3.18	0.58	0.15	2.84	2.63
La/Sc		1.32	4.61	5.66	2.34	1.26	7.92	8.43
Th/Cr		0.12	0.20	0.85	0.08	0.06	0.06	0.03
Y/Ni		4.83	1.01	21.55	0.95	7.26	13.44	44.33
Cr/V		3.08	0.88	0.67	0.87	0.33	–	–
Zr/Sc		9.83	25.03	23.30	16.39	24.63	45.52	96.98
Hf/Sc		0.35	0.74	0.80	0.47	0.59	1.28	2.90

** — ppb; **<d.l.** — below detection limit